ARTICLE

Thermodynamics of Nanocrystal-Ligand Binding Through Isothermal Titration Calorimetry

Received 00th January 20xx,
Accepted 00th January 20xx

DOI: 10.1039/x0xx00000x

Andrew B. Greytak,*[a] Sakiru L. Abiodun, Jennii M. Burrell, Emily N. Cook, Nuwanthaka P. Jayaweera, Md Moinul Islam, and Abdulla E Shaker

Manipulations of nanocrystal (NC) surfaces have propelled the applications of colloidal NCs across various fields such as bioimaging, catalysis, electronics, and sensing applications. In this Feature Article, we discuss the surface chemistry of colloidal NCs, with an emphasis on semiconductor quantum dots, and the binding motifs for various ligands that coordinate NC surfaces. We present isothermal titration calorimetry (ITC) as a viable technique for studying the thermodynamics of the ligand association and exchange at NC surfaces by discussing its principles of operation and highlighting results obtained to date. We give an in-depth description of various thermodynamic models that can be used to interpret NC-ligand interactions as measured not only by ITC, but also by NMR, fluorescence quenching, and fluorescence anisotropy techniques. Understanding the complexity of NC surface-ligand interactions can provide a wide range of avenues to tune their properties for desired applications.

1. Introduction

The ability to establish the identity and purity of nanocrystal samples with sufficient confidence to quantitatively predict chemical reactivity and physical properties, as is done routinely for molecular products, will have a transformative effect on synthesis, spectroscopy, and applications of many types of nanocrystals (NCs).[1–3] The challenge is that NCs in solution (colloidal NCs) are typically complex assemblies of a crystalline core and an interfacial layer that, given time, may exchange matter with the solution and with other NCs.[4] Changes in NC surface chemistry may strongly affect physical properties, subsequent surface reactions, and colloidal stability.[5–10] A very prominent example of such challenges is found in colloidal quantum dots, where surface chemistry can affect photoluminescence quantum yield (PLQY), and is critically important to many applications.[11,12] For example, in optoelectronic devices, surfaces influence the stability of quantum dot inks and transport in assembled films.[10,13] In bioimaging applications, surfaces influence brightness, nonspecific binding, and addition of specific targeting or sensing functions.[14] In photocatalysis and upconversion, surfaces mediate access of molecular reactants to NC surfaces for photochemical processes.[15–19] Accordingly, the chemistry of NC surfaces has been intensely investigated for many years in the context of semiconductor quantum dots (QDs)[14,20–25], metal oxides including magnetic nanoparticles (NPs)[26–30] and metal NCs.[31–43] In recent years, efforts by many groups have led to much greater understanding of the identity, surface density, and exchange equivalencies of organic ligands coordinating NC surfaces. These achievements put us in a position to define the thermodynamics of NC surfaces, which depends on well-defined initial and final states for representative reactions.

Experimental measurement of the thermodynamics of NC surfaces requires techniques that probe the extent of reactions at equilibrium. Techniques including NMR spectroscopy, fluorescence quenching, and fluorescence anisotropy (FA) are able to measure fractionation of molecules between surface and solution. An emerging technique is isothermal titration calorimetry (ITC), which measures the progress of binding interactions via the heat evolved as a reactant is titrated in. ITC is an established method in biochemistry,[44–51] but its applications to NC surfaces are emerging and have not yet been reviewed to our knowledge.

This Feature Article will focus on ITC as part of an expanding toolbox for studying the thermodynamics of NCs, with an emphasis on colloidal quantum dots. Via its sensitivity to the enthalpy change of reaction, it is able to resolve different types of binding sites and reveal information about inter-ligand interactions that may be difficult to access by other techniques. However, we also emphasize that the processes that are observable in ITC must also underlie the behavior of NCs in other measurements and in applications. Accordingly, the development of empirical thermodynamic models for ligand binding and exchange that can explain observed results, several of which we explore below, is applicable not only to ITC results, but also for interpreting results from the complete set of techniques including NMR.

It is possible to approach a description of NC surfaces from two opposing levels of detail. One approach is to start by considering what is known (or proposed) about surface

[a] Department of Chemistry and Biochemistry, University of South Carolina, Columbia, South Carolina 29208, USA. Corresponding author: Andrew Greytak greytak@sc.edu

structure at the atomic level, and attempt to predict observable behavior, introducing approximations as needed to deal with complexity. Given the diversity of crystal termination sites, ligand bonding arrangements, and non-covalent interactions among ligands and solvent, such models are computationally intensive. While some interactions can be calculated with precision, necessary choices about structures to consider[52] and the level of computational detail may result in such microscopic models retaining a large number of adjustable parameters that cannot be uniquely solved by comparison to experiment. The other approach – empirical thermodynamic models – starts by considering the simplest approximations, such as identical and independent sites for ligand binding, and introducing additional parameters (to describe different types of sites, or inter-ligand interactions) only to the extent that can be supported by reduction in residual error.[53,54] By limiting the number of adjustable parameters, it is often possible to obtain unique solutions that can be used to predict experimental results. The limitation is that the parameters obtained may represent a weighted average of more detailed microscopic factors, and it may be challenging to compare them to computational predictions. Despite these limitations, we argue that empirical thermodynamic models are extremely valuable in revealing NC surface chemistry that is useful in applications. In particular, if several sites with different microscopic structures cannot be distinguished in their reactivity under experimental conditions, it will not be possible to selectively modify them. Moreover, trends in empirical parameters across ligand structures, NC composition, or NC size can help to reveal the underlying microscopic factors at play. We will therefore emphasize empirical models in this article, while recognizing that a goal for the field must be to reconcile them with microscopic models guided by detailed knowledge of equilibrium structures.

Several groups have turned to ITC in recent years as a means to study NC surface chemistry.[51,55–66] It is able to detect ligand binding at a wide range of NC concentrations, which enables measurement of different binding constant ranges, and it is not limited to studying processes with distinctive NMR, UV-visible, or IR spectroscopic signatures.[55,67–69] A key feature of ITC is the ability to resolve sites with different binding constants based on different enthalpies of binding.[48,49,59,64,70,71] The value of ITC is multiplied if it can be combined with other techniques that independently monitor the extent of reaction, such as NMR, because these measurements can help to refine empirical models that account for the presence of multiple simultaneous reaction coordinates, and inter-ligand interactions on NC surfaces.[57,62,72]

Figure 1 illustrates the essential design and operation of ITC, originally described by Wiseman *et al.* as a method to study bioaffinity reactions.[44,48,49,73,74] A sample cell containing a solution of one reactant, typically a macromolecule such as a protein (or NC), is maintained at a setpoint temperature. This temperature control is achieved by maintaining a heat sink, separated from the laboratory by an adiabatic shield, at a temperature slightly below the setpoint. A feedback circuit continuously supplies power to the sample via a heater to keep it at the setpoint, while power is lost to the heat sink according to the difference in temperature. A syringe pump contains a solution of a second reactant, typically a ligand that may bind to or otherwise react with the first reactant, and is connected to the sample cell by a cannula.

When the syringe pump is advanced to combine the reactants, an exothermic or endothermic reaction may take place, causing a fluctuation in the power that must be supplied to the sample heater to maintain the sample at the setpoint temperature; when integrated over time, this difference in power represents the enthalpy change as the system is at constant pressure. To improve accuracy, a reference cell, filled with the same solvent, is maintained at a constant temperature and in contact with the sample cell, so that the signal is obtained from the difference in power supplied to the sample and reference cells to minimize their difference in temperature. In describing ITC data, the plot of differential power (heat rate) versus time is the thermogram (**Figure 1C**). In typical practice, the solution in the syringe is injected in a series of small steps with the same incremental volume; after each injection, the thermogram will show a deviation from the baseline value (more power for an endothermic process, less for an exothermic one), which relaxes back to the baseline as chemical and physical processes subside and the system within the sample cell returns to equilibrium at the new set of total concentrations. The peaks for each of the injections can then be integrated over time to obtain the total enthalpy change associated with each incremental step. In ITC parlance, the integrated data is the isotherm, and is usually the basis for further analysis.

The authors from left to right: Nuwanthaka P. Jayaweera, Emily N. Cook, Jennii M. Burrell, Andrew B. Greytak, Sakiru L. Abiodun, Abdulla E. Shaker, and Md. Moinul Islam. Graduate students NPJ and JMB and undergraduate student ENC are studying NC-ligand interactions in polar and aqueous environments. Graduate student SLA studies ligand exchange and stability in halide perovskite NCs. Graduate student AES is applying NC surface chemistry to optoelectronic devices, and graduate student MMI is investigating challenges in NC growth. Prof. Greytak has supervised research on purification, quantitative surface chemistry, and applications of NCs, particularly colloidal quantum dots, at the University of South Carolina since 2010.

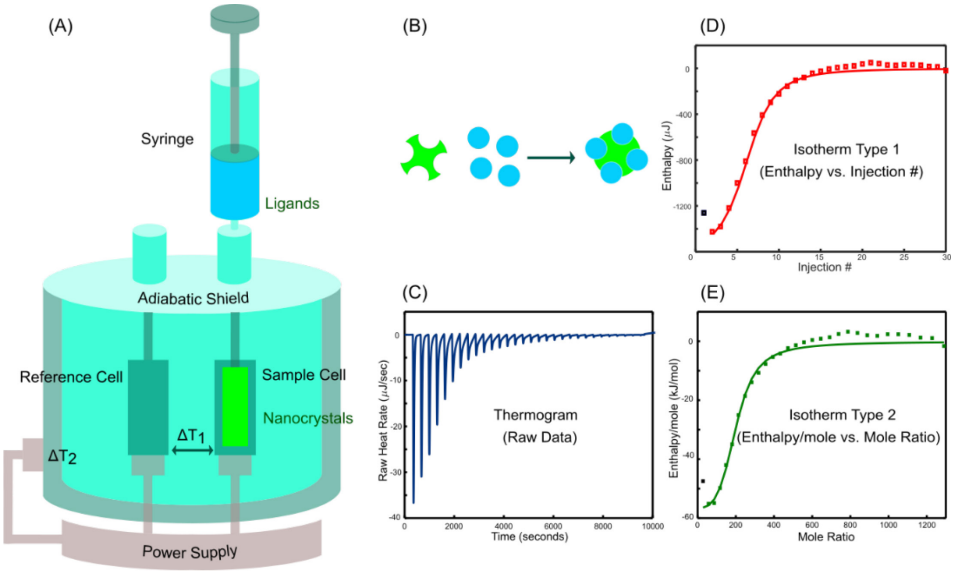

Figure 1. A, Schematic diagram of ITC instrument. B, Ligand association to a macromolecule (nanocrystal) with multiple binding sites. C, D, E, Baseline-corrected thermogram and integrated isotherm for a representative ligand exchange reaction performed on CdSe/ZnS quantum dots in aqueous buffer, with least-squares fit to an empirical model of identical, independent sites (Langmuir-Wiseman isotherm) giving N≈200 sites and ΔH≈−57 kJ/mol. Adapted with permission from Dunlap *et al.*, Ref. 56. Copyright 2022 American Chemical Society.

Isotherms can be plotted as enthalpy per injection number (**Figure 1D**), or, since the ligand concentration in the syringe is known, the enthalpy can be divided by the number of moles injected in each step. With knowledge of the macromolecule concentration in the cell, the enthalpy per mole injected can be plotted against the total ligand-to-macromolecule concentration predicted to be in the cell after each injection (**Figure 1E**). In modern instruments typical cell volumes are less than 200 µL, with the ability to detect heat signals less than 10 nJ per injection, and cell and syringe materials are designed for tolerance of a wide range of solvent and aqueous buffer conditions.

Basic data interpretation can be understood from a model where a macromolecule has some number of identical binding sites for a ligand that are independent, in that the equilibrium from binding of a ligand to any site does not depend on the occupancy of other sites. At the start of a titration in which the sites are initially empty, much of the ligand that is introduced will bind to vacant sites. The enthalpy change (ΔH) measured per mole of ligand added is thus similar to the standard ΔH for ligand association. However, as the sites become saturated, much of the ligand that is added remains in solution, and the heat measured per injection will diminish. The slope of the roll-off depends on the association constant K_a (or dissociation constant K_d=K_a^{-1}), with larger association constants resulting in a sharper transition. Least-squares fitting can obtain values for N, K_a, and ΔH. The biochemical literature describes the characteristics of this approach and ways to address cooperative binding, competitive binding, and sets of dissimilar sites.[45,46,48,49,51,70] ITC has been adapted to molecular binding in organic solutions,[75] and techniques have been devised for interpretation of continuous injections that may obtain parameters in less time in favorable circumstances.[76,77]

Particular challenges in the case of NC reactions studied via ITC are the large number of binding sites, heats of solution or mixing in organic solvents, polydispersity, and the need to maintain solubility of reactants and products in a homogeneous solution. Many of these challenges are endemic to any experimental approaches to thermodynamics of NC surfaces. In what follows, we will first describe common motifs for coordination of semiconductor NC surfaces by organic ligands, and some examples of reaction conditions for ligand exchange. We will then discuss complementary measurement techniques to study surface exchange reactions. Next we will examine empirical thermodynamic models in more detail, and steps towards an applicable microscopic picture. Finally, we offer some examples of the possibilities that await those who can develop improved control of NC-ligand binding.

2. Overview of surface coordination in nonpolar and polar solvent environments

Surface passivation is critical for the NC growth process and the colloidal stability of the post-synthetic product.[78,79] Importantly, surface passivation with either organic or inorganic ligands[80] aid in preserving physical and electronic properties of individual particles, while providing a structural feature that is tunable across a variety of solvent systems.

Surface passivation of NCs involves two main components: (1) direct interactions between the *binding motif* of the ligand and surface atoms of the NC and (2) steric or electrostatic interactions of the organic ligands extending into the solution

for colloidal stability. Structural components of the NC-ligand system, which can be altered for colloidal stability and functionality in a variety of environments, are schematically represented in **Figure 2**.

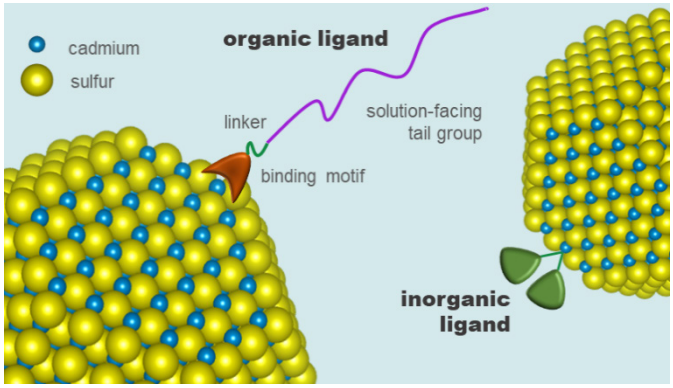

Figure 2. Typical organic ligand structural components including the binding motif, possible linker, and solvating tail group are illustrated. Additionally, inorganic ligands such as halides, are shown coordinating to a metal atom at the surface of a representative metal chalcogenide NC.

2.1 Representative binding motifs

Metal chalcogenides and pnictides. Colloidal NCs composed of polar-covalent compounds such as common II-VI, III-V, and IV-VI binary semiconductors are generally stabilized by a layer of ligands that coordinate the surface metals through covalent, ionic, or dative bonding.[1,81] Metal-rich surfaces with cationic character require charge-balancing that can be achieved by ligands with anionic, one electron donor ligands, referred to as X-type ligands. Neutral, two electron donor ligands that act as Lewis bases provide additional passivation for metal-rich surfaces and are known as L-type ligands. Electrophilic Z-type ligands, often metal complexes of that can be represented as MX_y, passivate under-coordinated chalcogen- or pnictogen-rich surfaces by acting as neutral electron acceptors. Structural examples of these binding motifs can be found below in **Figure 3.**

A model of charge neutrality in direct coordination of NC surfaces may be inaccurate: chalcogenide and pnictide NCs stabilized by only neutral ligands are difficult to find. Polar solvents can support dispersions of charged colloidal particles, and even in nonpolar solvents, stabilization by secondary electrostatic ligands or groups has been observed in samples where charge-neutral coordination had been previously proposed.[82] We have recently observed that histidine-based small-molecule ligands stabilize CdSe/ZnS core/shell NCs via both neutral binding of imidazoles, and X-type chloride binding facilitated by presence of a primary amine in the tail of the histidine-based ligands that contributes to the charge balance at the NC surface.[83]

Halide perovskite compounds. The binding motifs encountered with halide perovskite NCs (e.g. $CsPbX_3$) differ from what has been observed in polar-covalent NCs due to their more strongly ionic character. Work by several groups[84–87] has indicated that $CsPbX_3$ NC surfaces can be represented as an inner core, a final PbX_2 plane, and a terminal A^+X^- layer in which Cs^+ and/or X^- ions may be substituted by ligands, as illustrated in **Figure 4**. Among several ligands that have been investigated, primary, secondary, tertiary, and quaternary alkylammonium ions that can substitute the A^+ sites, and various halide, sulfonate, or thiocyanate counterions that may substitute the X^- sites, were found to be effective. The absence of exchangeable protons on quaternary ammonium ligands helps to prevent detachment of the ligand from the NC surface, enabling improvement in PLQY and stability toward purification, including by gel permeation chromatography (GPC).[88,89]

2.2 Ligand architecture and colloidal stability

Ligands provide colloidal stability by controlling intermolecular interactions between surface ligands, solution components and other NCs present. These are the primary function of the linker and tail portions of organic ligands as shown in **Figure 2**. The architecture of surface ligands describes how solution-facing structures are connected to the binding motifs, and may encompass alkyl chains in small molecules, oligomeric structures with several binding motifs, and polymer sequences that include multiple binding motifs. These aspects of ligand design and several prominent examples are illustrated in **Figure 3**.

In general, the ideal ligand shell for a particular environment provides a balance of weak attractions between ligand and solvent molecules to maintain suspension, while providing a macroscale steric repulsion that keeps the inorganic cores from physically interacting and diminishing their size-specific physical properties. The overall thermodynamic picture of the system includes contributions from direct binding interactions of the binding motifs, and also enthalpic and entropic contributions from ligand-ligand and ligand-solvent interactions that can be strongly influenced by differences in architecture.[61,90,91]

Stabilization in hydrophobic solvents. NC syntheses typically involve the use of nonpolar, high boiling point solvents to initiate crystal nucleation and growth at high temperatures.[92–97] The resulting NCs produced by these high-temperature growth methods typically have ligands with nonpolar linker/tail groups coordinated to the surface. A commonly used passivating ligand is oleic acid, with an 18-carbon chain extending from the carboxylate binding motif. Weakly attractive London dispersion forces are at work here between hydrophobic ligands and solvent molecules, keeping the particles stably suspended, while providing a collective steric repulsion between individual NCs.

Stabilization in polar solvents. At the surface of NCs, charge balancing interactions that occur between the surface atoms of the NC and ligand binding motif, or electrostatic associations with ions in solution, are just one part of the story. Beyond these interactions at the surface, the outer components of the ligand architecture may take part in many different types of attractive interactions in polar and aqueous environments. Polar ligand architectures may include molecules functionalized with carbonyl groups, hydrogen bonding donors and acceptors, and zwitterionic moieties which all contribute toward increased stability in polar-organic and aqueous environments. Common ligand architectures used in polar and aqueous environments

are highlighted in **Figure 3** and range from small molecules to zwitterionic and polymeric architectures.

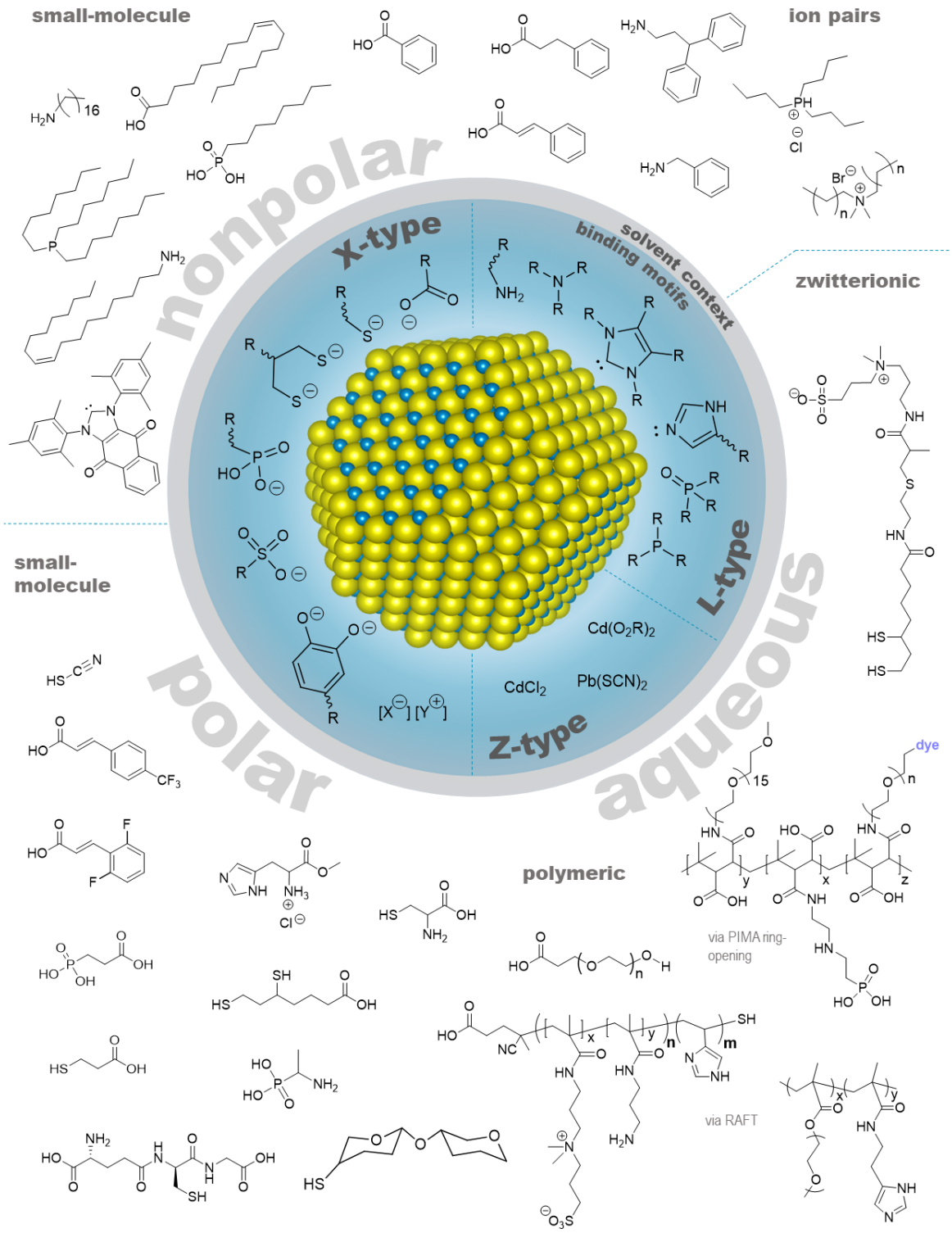

Figure 3. Surrounding a representative core are common binding motifs categorized as X-, L-, and Z-type. Examples of ligand architectures common to different solvent contexts are featured in the outer sections, including nonpolar [Refs: 98 99 100 101 102], polar and aqueous [Refs: 28, 103 104 83 105 106 107 108]. The examples listed are primarily used with metal-chalcogenide, metal-pnictide, and lead halide perovskites.

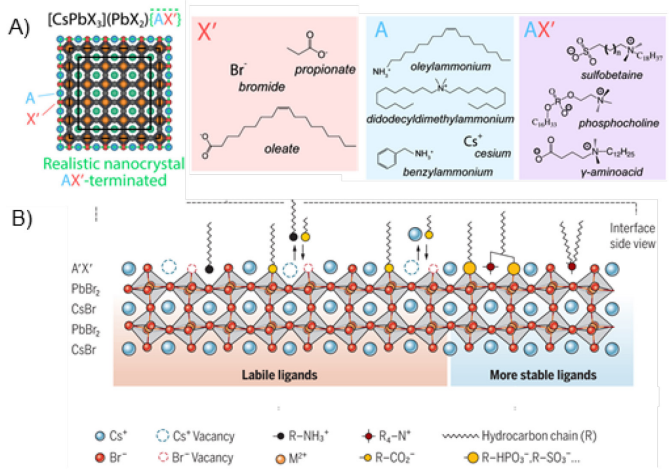

Figure 4. Surface termination and ligand binding motifs for halide perovskite NCs. Part A is adapted with permission from Bodnarchuk *et al.*, Ref. 85 (CC-BY-NC-ND 4.0). Part B is adapted with permission from Ye *et al.*, Ref. 109 (CC-BY-4.0).

Because of their robust size-tunable photophysical properties, many studies have focused heavily on adapting the surface chemistry of NCs for applications in aqueous solutions toward the goal of applying these properties to diagnostic bioimaging and biosensing pursuits.[11,20] Additionally, NC-based electronic inks often depend on solution-phase ligand exchange with small molecules that require stabilization in polar organic solvents as they lack the steric stabilization capabilities of typical native ligands.[110,111] For example, 3-mercaptopropionic acid (MPA) is one of the most explored short organic ligands for PbS NCs.[112,113] Its carboxylate group can help to confer solubility in polar liquids via hydrogen bonding and/or charge stabilization. However, stable solutions in polar organics have required the addition of halide ligands balanced by ammonium counterions. To form *p*-type PbS inks without halides, we paired MPA with a weakly coordinating and basic solvent, benzylamine, achieving inks stable over a period of weeks or longer.[10]

Polymeric ligands. The multiply-binding character of copolymer architectures with separate binding and solvating monomer residues[106,107,114–118] offers increased colloidal stability in polar-organic and aqueous media for many types of semiconductor and metallic NCs, when compared to small molecules with only one or several binding motifs.

Compared to polymer encapsulation strategies that preserve the native ligand set,[119–121] multiply-binding ligands afford smaller hydrodynamic sizes, while suppressing nonspecific binding of NCs to biological molecules and surfaces. The solvating units may be polar polymeric groups such as poly(ethylene glycol) (PEG),[122,123] zwitterionic groups such as sulfo- and carboxybetaine,[124–126] and charged groups like carboxylates or quaternary amines.[122,127] Copolymer ligands can be prepared by copolymerization of separate binding (e.g. imidazole, thiolate, catechol) and solvating/linking monomers that interact directly with the environment, or by partial modification of homopolymers.[106,107,114,124,128,129] Poly(isobutylene-*alt*-maleic anhydride) (PIMA) is frequently used as a polymer backbone for partial modification due the ease and versatility with which the maleic anhydride rings can be functionalized with binding or solvating architectures.[130] Alternatively, reversible addition-fragmentation chain transfer (RAFT) polymerization has been used to design copolymers, including block copolymers. The terminal ends of the backbone and/or the solvating groups may be further modified with a spectroscopic handle, linking sites for bioconjugation reactions, or polymer brushes for additional steric stabilization.[107,114,128,131,132]

Polymer architecture appears to be important: block copolymers with synthetically specified sequences enable "binding patches'' that lead to strong binding and high surface coverage.[133,107,106] In a direct comparison, we found that block copolymers were superior both in terms of stability and surface protection.[106] However, random or alternating binding and solvating residues can lead to the smallest hydrodynamic sizes.[134] Giovanelli *et al.* have shown that polymeric ligands also offer kinetic stability (**Figure 5**).[135] However, the thermodynamic implications of copolymeric ligand coatings in these environments have not yet been explored fully.

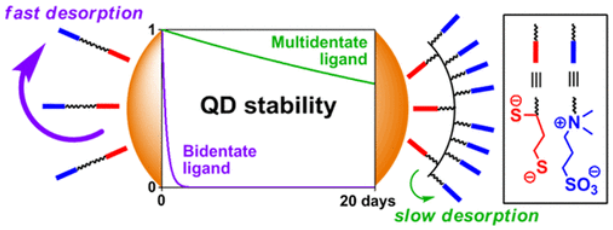

Figure 5. Polymeric ligands offer enhanced stability, in part through slower desorption rates compared to small molecules, detected for CdSe/CdS/ZnS NCs using fluorescently labeled ligands. Reprinted with permission from Giovanelli *et al.*, Ref. 135. Copyright 2012 American Chemical Society.

2.3 Symmetry concerns

Nanocrystal core structures are typically represented by a truncated form of a bulk crystal phase, a polycrystalline structure in which periodic domains are joined by grain boundaries, or quasi-periodic structures built around a singular point such as in some icosahedral metal NC structures. In each case, the limited set of symmetry operations that can be applied to the core structure will generally require that their surfaces present at least several different types of coordination environments associated with different lattice planes, edges, and corners. These environments may have different spacing for coordination sites, different bonding geometries, and/or different charge balance requirements. Additional complexity results from NC shape, size, and local curvature,[136] which affect the volume available to ligands anchored at surface coordination sites.[60,137,138] As a result, we expect that a complete thermodynamic description of NC-ligand interactions should include multiple types of sites.[4,61,139,140] Experimental measurements may or may not present sufficient evidence to describe such differences; however, if reactivity at different sites can be resolved, it opens the possibility of using the NC core as a scaffold for designing complex structures, or for using ligand mixtures to direct NC shapes.[141,142]

For example, the dominant binding sites for octahedral PbS NCs smaller than 3 nm are polar (111) facets. However, as the size of PbS NCs increases, the octahedral vertices become more truncated, forming a cuboctahedral shape therefore changing the dominant sites to polar (111) and neutral (100) facets.[143]

2.4 Ligand exchange and phase transfers

Deliberate ligand exchange procedures are vital in colloidal chemistry because they allow NC synthetic considerations to be separated from optimization of surface interactions, so that narrowly distributed physical properties can be achieved in any desired phase. [144–147] Moreover, well-defined ligand exchange reactions are needed to make experimental measurements of NC-ligand thermodynamics.

A significant amount of research has been conducted over the years to understand the types of reactions that take place between NC surface atoms and various ligand types.[101,146,148,148–152]

Nonpolar/nonpolar ligand exchanges. The exchange of native hydrophobic ligands for different nonpolar architectures can be advantageous in stabilizing quantum dots with high PLQY for luminescence applications and fundamental investigations.[67,153,154] Nonpolar solvents do not easily support separated ions, which simplifies descriptions of ligand exchange via charge balance.[155] Consequently, nonpolar solvents have been the context for many fundamental studies of ligand exchange reactions. In the case of chalcogenide and pnictide NCs, ligand exchange reactions have been interpreted through schemes such as those presented by Owen, reproduced in **Figure 6**.[156]

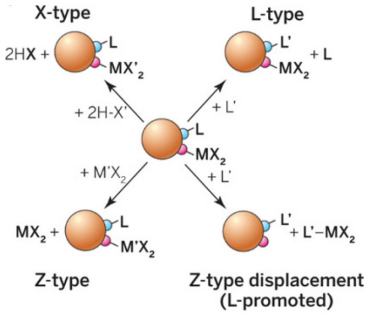

Figure 6. Representative ligand exchange reactions maintaining charge balance on polar-covalent NC surfaces. From Owen, 2015, Ref. 156. Reprinted with permission from AAAS.

While a very useful starting point, overly simplified application of these schemes may give an incomplete picture of some real NC ligand exchange reactions. For example, diprotic phosphonic acids may displace multiple carboxylates, and some compounds can participate in multiple binding modes (e.g. X-type or L-type) depending on protonation state as illustrated in a recent investigation of InP clusters by Ritchhart and Cossairt (**Figure 7**).[157] Reactions among ligands with hydrophobic tails can often be carried out in monophasic solutions in nonpolar or weakly polar solvents, facilitating thermodynamic investigation via ITC, as well as other thermodynamic characterization techniques.

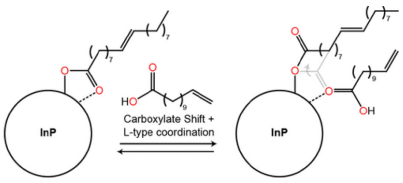

Figure 7. Scheme representing X-type coordination of carboxylate and L-type coordination of carboxylic acid on atomically-precise InP nanoclusters, as evaluated from NMR. Reprinted with permission from Ritchhart and Cossairt, Ref. 157. Copyright 2019 American Chemical Society.

Nonpolar/polar ligand exchanges. Insulating native ligands are often exchanged for more compact and/or conductive ligands to decrease interparticle distance and facilitate charge transport between NCs in thin films for increased electronic performance.[99,100,103] This often entails a change to a more polar organic solvent in which the native ligand coating may not provide colloidal stability, which poses additional challenges for conducting ligand exchange reactions. Solid-state ligand exchange has historically been applied most widely in the exchange of native nonpolar ligands for more compact ligands in assembled NC films for electronics, but is inefficient compared to preparation of stable, solution-phase inks. Exchange of nonpolar ligands for polar architectures may involve either monophasic or biphasic solvent systems. Recent work in our group has highlighted the successful biphasic solution-phase exchange of PbS and ternary $AgBiS_2$ NCs to form inks for single deposition thin film fabrication.[10,158] Studies in polar organic solvents may also aid in prototyping surface chemistry that is aimed at biomedical applications in water.[83]

Nonpolar/aqueous ligand exchanges. Ligand exchanges to install hydrophilic coatings on NCs synthesized in hydrophobic solvents are commonly achieved via biphasic reactions with ligands in aqueous solution, or by co-dissolving NCs and ligands in homogeneous polar organic solutions followed by transfer to water or aqueous buffers.[20] Historically, many of these reactions have involved large excesses of hydrophilic ligands.[159] For ITC studies, it is important to identify reactions that can be conducted in a homogeneous phase with controlled stoichiometry. For thermodynamic studies of ligand coordination in buffered aqueous solution, an initial exchange with a ligand that supports colloidal stability in water, and yet is labile toward exchange with more strongly binding ligands of interest, may be advantageous.[56,160,161] Control of pH and ionic strength is critical, as these will modulate the protonation state of binding motifs and solution phase ligands, and influence charge balance considerations.

3. Measurement techniques to quantify NC-ligand binding

An expanding toolbox of measurement techniques that can be used to study thermodynamics of NC-ligand binding are explained below. While the focus of this Feature Article is ITC, it is important to explore additional techniques that can also be used to probe NC-ligand interactions. We are particularly interested in methods that do not require separation of NC-

ligand complexes from solution, but can be used *in situ* to probe reactions at equilibrium. These methods can be used individually or in a complementary manner, and software packages are available that are designed to predict the results of multiple types of measurements using the same thermodynamic model.[162] **Figure 8** illustrates four such techniques that we will discuss below.

3.1 NMR spectroscopy

NMR techniques (**Figure 8A**) such as ^{1}H NMR, diffusion ordered spectroscopy (DOSY) and nuclear Overhauser effect spectroscopy (NOESY) have proven to be very reliable tools for elucidating the identity of ligands that are binding to NC surfaces, molecular-level structural relationships between neighbouring ligands, and binding thermodynamics.[27,149,163,164] The difference in the position and line shape of the ligand NMR signals can frequently be used to differentiate ligands that are free in solution from those that are bound to the NC surface. In the case that the exchange occurs slowly on the NMR relaxation timescale, the spectrum may be represented by a linear combination of resonances for bound and free forms. Broadening is generally observed in the resonances of nuclei localized to the surface of the NCs compared to those free in solution, and this is attributed to the heterogeneity in the size and shape of the NCs, decrease in spin-spin relaxation time and/or slow tumbling of the large NCs.[164–166] As long as steps are taken to provide sufficient relaxation delay between measurements, integrated signals are proportional to concentration, and by using internal or external standards, ligand concentrations can be estimated. When the NC concentration can be determined (from calibration curves, or analytical chemistry methods such as total elemental composition[167] or osmometry[168]), ligand to NC ratios can be evaluated. Thus, by relating changes in bound ligand populations to concentrations of ligands in solution, association or exchange equilibrium constants can be determined. By running the experiments at different temperatures and using van't Hoff analysis (In K vs T^{-1}), ΔH and ΔS can be obtained.

A key requirement for NMR is one or more unique spectroscopic handles whose resonances can be distinguished from other materials in the sample. Dempsey's group used probe molecules with terminal alkene functions that can be distinguished from oleate species and alkane background to examine ligand exchange of oleate capped CdSe NCs with carboxylic acids, phosphonic acids, and thiols.[169] Therein, they found undec-10-enoic acid to undergo an exchange with oleate with an equilibrium constant K_{ex} of 0.83, whereas K_{ex} for phosphonic acid and thiol-terminated ligands were too large to measure.[169] The same group used ^{1}H NMR to unravel the exchange mechanisms and thermodynamics of exchange of oleate capped PbS NCs with thiol-based ligands.[147] In a similar vein, Brutchey's group employed the use of ^{1}H NMR to quantify the thermodynamics of ligand exchange on $CsPbBr_3$ quantum dots.[86] Therein, they measured K_{ex} for the exchange of native oleate with undecanoic acid, and for the exchange of the oleylamine with undec-10-en-1-amine. Despite the many capabilities of the technique, there remain significant limitations in using NMR alone to elucidate the thermodynamics of ligand exchange on NCs surface. For example, NMR requires high NC and ligand concentrations to obtain signals that can be reliably integrated against background. This is a particular limitation in measuring large association or exchange constants where free ligand concentrations are low over a wide range of surface occupation states. Sometimes, exchange between bound and free populations is too fast to produce distinct signals.[147] In such cases, we have employed variable temperature NMR[83,138] and DOSY[10,89,170] to identify ligands that are interacting with the NC surface, but these approaches may be insufficient to yield reliable equilibrium constants.

3.2 Fluorescence Anisotropy

Fluorescence anisotropy (FA) relies on exciting a fluorophore whose transition dipole undergoes rotational diffusion.[53] It can be used to measure adsorption of a fluorescent probe molecule to the NC surface. As illustrated in **Figure 8B**, a free ligand in solution will exhibit low anisotropy r due to constant free rotation of the molecule in solution. However, when bonded to macromolecule or NCs surface, r increases due to increased local viscosity from interaction with other molecules bound to the surface, and slow rotational diffusion of the macromolecule as a whole. This technique has been extensively applied to detect and measure binding interactions in biomedical fields including drug discovery.[171–174] FA has been used to measure the dynamic properties of the ligand shell on the surface of CdSe NCs [175] as well as to measure the dynamics of the self-assembled monolayer on gold NC surfaces.[176]

The advantage of using FA to elucidate the binding strength of ligands to macromolecules is that it only requires a small amount of ligand and macromolecules and can be automated for fast measurement of large number of samples. The signal is intrinsically related to the ratio of bound and free populations, and it can be designed to probe low and high K_a values. However, shortcomings of using FA include the necessity of a fluorescent ligand, and the saturation of fluorescence signals due to self-quenching at high fractional occupation of surface sites, as well as fluorescence background from NCs themselves.

3.3 Fluorescence Quenching

Just like FA, quenching of a fluorophore due to complexation can be used to measure the binding affinity of a ligand to a macromolecule.[53] Quenching can be classified as dynamic or static. Dynamic quenching of a molecule occurs when there is energy or electron transfer between the donor and the acceptor species as a result of collisions within the donor decay lifetime, causing a decrease in average lifetime[177] that varies with acceptor concentration. However, static quenching occurs due to a quencher (ligand) that is already bound to a donor fluorophore (macromolecule), resulting in emission from an equilibrium distribution of NC-ligand complexes as represented in **Figure 8C**. Thus, static quenching is more useful in assessing the binding strength of a ligand to a macromolecule. In measuring the binding strength of a ligand using PL quenching, a quencher molecule is titrated into a solution of fluorescent macromolecules and the intensity change (final fluorescence intensity) upon complex formation is then monitored. By monitoring the concentration of the quencher that is titrated into the macromolecule and the resulting reduction in fluorescence intensity, the binding affinity of the quencher to the fluorophore macromolecule can be estimated. Fluorescence quenching can be performed in continuous-wave or time-resolved modes. It is well suited to quantum dot NCs

due to their intrinsic PL, and has been used in some of the earliest thermodynamic investigations of quantum dot-ligand interactions.[178–183] Mulvaney and Bullen[179] used this technique to estimate the adsorption equilibrium constant of different amines and thiols on the surface of CdSe NCs. Munro *et al.*, also estimated the K_a for amines on the surface of CdSe NCs to be on the order of 10^6 M^{-1} (lower limit) using PL quenching.[180] Despite the wide accessibility of this technique,[182,184] the use of PL quenching to measure the binding of ligands to NC surfaces is challenging because the reduction in PL intensity associated with ligand binding is strongly ligand-dependent and is not necessarily proportional to fractional ligand coverage over a wide range. As such it is best suited to probing a small number of vacant binding sites on NCs stabilized by other ligands[178,182,185] or uptake of metal ion quenchers[184] rather than complete ligand exchanges.

3.4 Microscale Thermophoresis (MST)

MST (illustrated in **Figure 8D**) is another technique that can be used to estimate the binding of ligands to a fluorophore-labelled (or naturally fluorescent) macromolecule.[186,187] Designed as an approach to measuring bioaffinity interactions in conditions that are as close to physiological as possible, it is marketed as a competing technology to ITC. A sample consisting of a homogeneous mixture of macromolecule and proposed ligand is locally heated with a focused infrared laser, while fluorescence is probed via UV or visible excitation. The heating tends to cause macromolecules to diffuse away from the focal point (thermophoresis), causing a reduction in fluorescence that may be augmented by temperature-related changes in brightness. Both of these properties may change when a ligand is bound to the macromolecule: for example, the mobility is diminished by an increase in hydrodynamic size. The details of the response to local heating are not necessary to determine a binding constant: instead, the experiment is repeated on a series of samples prepared with a wide range of ligand and/or macromolecule concentrations. Only very low sample volumes are needed, and can be prepared in disposable capillary tubes. This feature avoids many concerns with sample contamination and in principle permits almost any solvent to be used including strictly air-free preparation and measurement. This technique has been used to study binding affinity in various biological examples[188–190] but its applications to NCs is still limited. Compared to ITC or NMR, MST may face difficulties in resolving complex thermodynamic models due to the limited number of concentration points. Also, changes in thermophoresis are related to changes in hydrodynamic size that might not be very significant for small molecule exchange at NC surfaces. However, the intrinsic fluorescence of quantum dots could make them easy to study with MST, or even make them usable as part of a labelling system for studying affinity interactions between biomolecules.

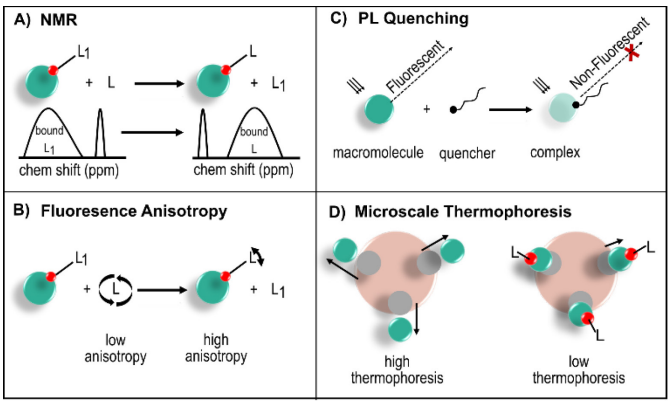

Figure 8: Several measurement techniques for NC-ligand thermodynamics. We note that panel A represents the limit of slow exchange on the NMR measurement timescale.

3.5 Comparison with ITC

Compared with the above techniques, ITC is unique in that it can simultaneously determine all binding parameters (equilibrium constant, enthalpy change ΔH, reaction stoichiometry, Gibbs free energy ΔG, and entropy change ΔS) in a single experiment, can probe a wide range of binding constant values, produces a large number of isotherm points supporting evaluation of complex models, and does not require specific spectroscopic handles. ITC is also non-destructive in that samples may be recovered for spectroscopic analysis. However, the technique does pose some unique challenges in that because it measures all sources of enthalpy change, it is sensitive to heats of mixing and dilution (including mixing of organic solvents with different amounts of adventitious water), thus requiring careful attention to background runs. Sample quantities are typically smaller than those required for NMR, but much greater than required for optical spectroscopy. It is difficult to prepare samples in a strictly air-free manner, though the small diameter of sample and reference loading tubes limits exposure. Analysis of ITC data requires consideration of the volume displaced from the cell by each injection (as the cells are typically overfilled to improve signal quality), which is handled by built-in software but requires attention in custom analysis.

3.6 Preparation of NC samples for reliable measurements

Thermodynamic measurements depend on knowledge of reagent concentrations. For colloidal NCs, this means developing measurements for, and control of, total ligand and NC concentrations. A variety of purification techniques can be used to separate NCs and strongly-bound ligands from solution-phase components.[191,192] Total concentrations of ligands retained by NC samples can frequently be obtained from NMR or ultraviolet-visible spectroscopy, or from thermogravimetric analysis. Based on such analysis, we have found gel permeation chromatography (GPC) to be an especially helpful technique for obtaining samples with reliable properties such as native ligand density and ligand exchange equivalency,[191,193] and it has also been adopted by other groups.[157,194,195] Assignment of NC concentrations can be more problematic because it typically requires knowledge of both the total amount of compound and the average particle volume. The average particle volume can in

principle be assigned from the distribution of particle diameter or projected areas as determined, for example, by microscopy.

In practice, especially for quantum dots, NC concentrations are frequently assigned from calibration curves that assign total concentrations and/or size based on electronic (UV-vis-NIR) absorption spectra. For example, calibration curves for size and concentration are available for wurtzite (WZ) CdSe,[168,196–198] WZ CdS,[198] zincblende (ZB) CdSe and CdS,[199] tetragonal $CuInS_2$,[200] $CsPbX_3$,[201,202] CdTe,[198,203,204] PbSe,[205,206] PbTe, PbS,[207,208] InP, InAs,[209] and ZnSe.[210]

4. Thermodynamic models

In what follows, we will describe empirical thermodynamic models that are suited to describing the binding of ligands to a macromolecule M (here, the NC) with a multitude of potential binding sites. These models, some of which are highlighted in **Figure 9**, can be used to describe and predict the results of ligand exchange reactions while remaining agnostic as to the identity or detailed structure of the actual surface coordination and ligand conformation environments. However, independent data on structure of NC or NC-ligand complexes may provide constraints on empirical model parameters that make the results more likely to be useful over a range of NC sizes and ligand scope.

4.1 Langmuir

The starting point for thermodynamic analysis of ligand binding is the biomolecular association of a ligand L to some site S to form a ligand-site complex SL. This can be described by the following chemical equation, which defines K_a:

$$\mathbf{S+L=SL} \qquad (1a)$$

$$\boldsymbol{K_a} = \frac{[\mathbf{SL}]}{[\mathbf{S}][\mathbf{L}]} = \frac{\boldsymbol{\theta}}{(\mathbf{1}-\boldsymbol{\theta})[\mathbf{L}]} \qquad (1b)$$

Where [S] and [SL] describe the molar concentration of free and occupied sites. This simple model is widely used to describe binding of ligands to biomacromolecules (though often the dissociation constant K_d=1/K_a is used to describe the equilibrium, as it is numerically equal to [L] at 50% occupancy, *i.e.* when [S]=[SL]). When attempting to identify K_a from a titration experiment, the number of sites per macromolecule, N, might not be known. In the case that all sites per macromolecule are identical and their binding equilibria are independent (Figure 9A), we arrive at a model very similar to the Langmuir model for gas adsorption at surfaces, in which the fractional occupation (probability of being occupied by a ligand at any time) ϑ of all sites simply depends on the free ligand concentration [L] and K_a. This is known as the Langmuir isotherm. In titration experiments, it is frequently the total concentrations of ligand ([L]t = [L]+[SL]) and macromolecules $[M]_t$ (i.e. the NC: in what follows NC concentrations will be referred to as [M] for consistency with biochemical literature) that are controlled. Allowing the possibility of some number of identical, non-interacting sites N per macromolecule, the total concentration of sites is given by $N[M]_t$, and in such a case [L] and ϑ can be obtained from a quadratic equation given K_a. The

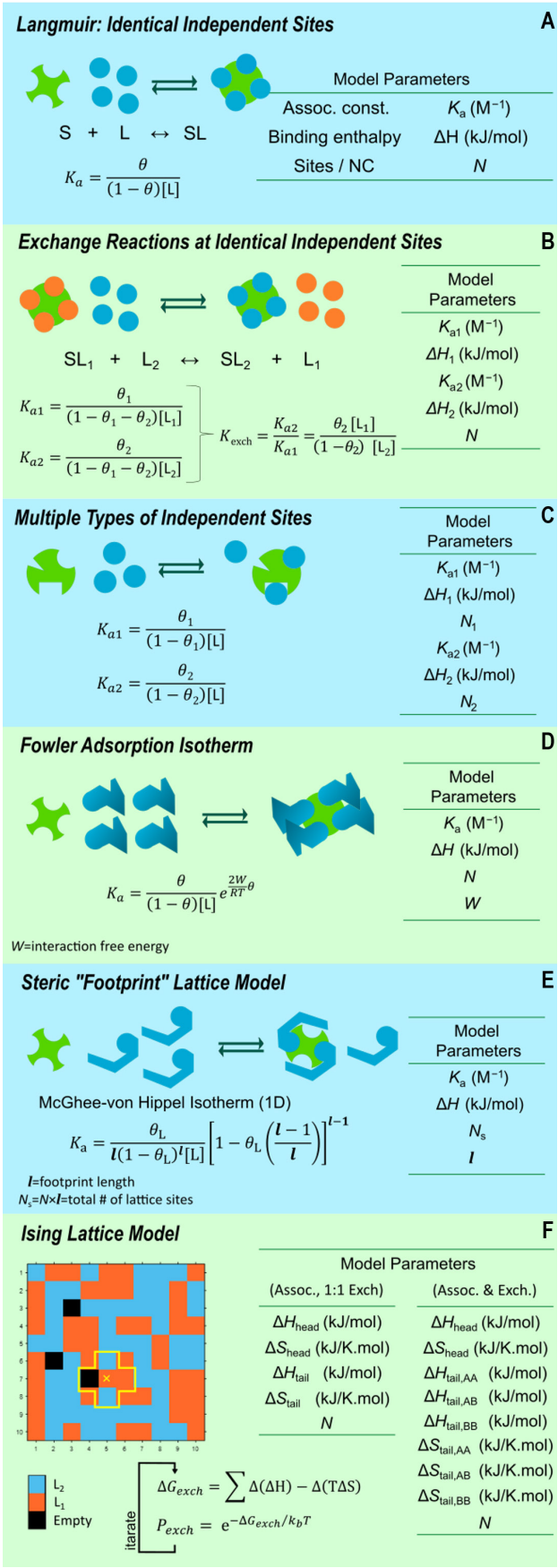

Figure 9. Common empirical thermodynamic models for NC-ligand interactions.

form when ϑ is expressed as a function of $[L]_t$ is known as the Langmuir-Wiseman isotherm,[44] which is frequently encountered in ITC. Langmuir-Wiseman isotherms have a characteristic shape determined by the Brandts "*c* parameter" $c=K_aN[M]_t$, while ITC can additionally provide a value for the enthalpy ΔH per site. When $c > 1$, unique values for N, K_a, and ΔH can often be resolved from fits to experimental data; curve shapes and analysis including at low *c* have been reviewed.[211,212]

The Langmuir model is a useful starting point for describing ligand binding to NCs because of its simple form, its ability to describe binding to a large number of sites, and because more complex ligand exchange models can often be reduced to behavior very similar to the Langmuir model in certain limits.

Use of the Langmuir isotherm is routine in ITC measurements of noncovalent adsorption of proteins to nanoparticles.[51] It has also been applied to the earliest ITC studies of L-type ligand coordination to NC surfaces by Jones's group[55] and ours.[67] Using ITC in toluene, we demonstrated that trioctylphosphine (TOP) and oleylamine can adsorb to vacant sites on purified, oleate-capped WZ CdSe/CdS core/shell NCs with K_a~10^4 M^{-1}, whereas trioctylphosphine oxide (TOPO) showed negligible binding (**Figure 10**). Prior to this, Bardeen and Tang's groups found that a Langmuir isotherm described adsorption of carboxylic acids to oleate-capped CdS NCs using fluorescence quenching.[178] However, many NC surface reactions entail exchange, not merely adsorption, and detailed investigations are revealing evidence of multiple types of sites and/or interactions. Before considering more complex models for NC-ligand binding, it is worth examining the most general approaches to describing binding at multiple sites, which has been explored at length in biochemical literature.

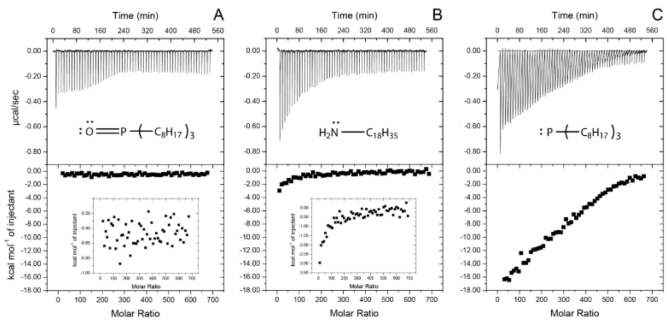

Figure 10. Titration of several nucleophiles into wurtzite CdSe/CdS core/shell NCs with pre-existing $Cd(oleate)_2$ coordination in THF solution at room temperature. Despite a low *c* parameter in this experiment, exothermic association of oleylamine and TOP can be seen with K_a~10^4 M^{-1}, in contrast to TOPO. Adapted with permission from Shen *et al.*, Ref. 67. Copyright 2015 American Chemical Society.

Beyond Langmuir: general case of multiple sites. The most general approach makes use of a "binding polynomial" that is the partition function for the macromolecule in the system.[70] It relies on a set of cumulative, or total, association constants β_i that describe the formation of complex(es) with a certain number *i* of ligands bound:

$$M + iL = ML_i \qquad (2a)$$

$$\boldsymbol{\beta_i} = \frac{[\mathbf{ML_i}]}{[\mathbf{M}][\mathbf{L}]^i} \qquad (2b)$$

The concentrations of all these possible complexes must simultaneously be in equilibrium with the free concentrations [M] and [L]. The binding polynomial *P* is defined as:

$$\boldsymbol{P} = \sum_{i=0}^{N} \frac{[\mathbf{ML_i}]}{[\mathbf{M}]} = \mathbf{1} + \sum_{i=1}^{N} \boldsymbol{\beta_i}[\mathbf{L}]^i \qquad (3)$$

where N is the largest possible number of ligands bound, and it can be used, given values for β_i and the free ligand concentration [L], to obtain the fractional populations of free M and each ML_i complex at equilibrium. The total fractional occupancy ϑ, now representing the total concentration of bound ligands $[L]_b$ divided by the total concentration of sites $N[M]_t$, is given by:

$$\boldsymbol{\theta} = \frac{[\mathbf{L}]_b}{N[\mathbf{M}]_t} = \frac{1}{N}\frac{\sum_{i=1}^{N} i[\mathbf{ML_i}]}{[\mathbf{M}]+\sum_{i=1}^{N}[\mathbf{ML_i}]} = \frac{1}{N}\frac{\sum_{i=1}^{N} i\boldsymbol{\beta_i}[\mathbf{L}]^i}{\boldsymbol{P}} \qquad (4)$$

In an ITC experiment, we know $[L]_t$ and $[M]_t$ at the conclusion of each titration step. Through conservation of matter, we can write:

$$[\mathbf{L}]_\mathbf{t} = [\mathbf{L}] + \boldsymbol{N}[\mathbf{M}]_\mathbf{t}\boldsymbol{\theta} = [\mathbf{L}] + [\mathbf{M}]_\mathbf{t}\frac{\sum_{i=1}^{N} i\boldsymbol{\beta_i}[\mathbf{L}]^i}{\boldsymbol{P}} \qquad (5)$$

Multiplying by *P* produces a polynomial of order N+1 that can in principle be solved analytically or numerically to find [L] at equilibrium for any set of β_i. By assigning an average ΔH_i for each set of complexes ML_i, the entire isotherm can be simulated and compared with experiment.

This approach can completely account for interactions and differences among sites: the β_i's can be expressed as a product of incremental association constants K_i describing the addition of each additional ligand, which may naturally depend on what sites are already occupied. However, the set of K_i's is not unique as they may depend on the order in which sites are filled. The connection to the Langmuir isotherm, and deviations associated with interactions, can be seen through microscopic association constants k_i describing the association of a ligand to a particular site *i* in the absence of any other interactions. The β_i can then be described in terms of the various combinations of site occupancy, with an interaction parameter describing cooperative or anti-cooperative behavior. For identical and independent sites, k_i is simply the Langmuir association constant K_a and $\beta_N=k^N$. Binding to two identical, but interacting sites finds $\beta_1=2k$ and $\beta_2=\kappa k^2$ where k is the microscopic association constant for either site and κ is an interaction parameter; $\kappa>1$ for cooperative binding, $\kappa<1$ for anti-cooperative, and $\kappa=1$ for the independent case. The approach is well suited to small numbers of interacting sites such as metal ions binding to peptides or synthetic cryptand macrocycles,[45,50,213] but it should be clear that the complete description of large numbers of sites, as found on NC surfaces, according to the binding polynomial approach is mathematically unwieldy (requiring high-order polynomials) and has a parameter set that is far too large to be resolved experimentally.

A simplified approach to considering cooperativity is found in the Hill equation, originally developed to interpret O_2 binding to hemoglobin and commonly encountered in biochemical

literature. Only the completely occupied and unoccupied cases are considered, equivalent to retaining only the terms with *i* equal to a "Hill parameter" *n* in Equation 5. In practice, *n* is allowed to vary with *n*>1 representing cooperativity. Here, we emphasize that the Hill equation has substantial limitations in describing interactions with multiple sites on NCs. Most importantly, the Hill parameter *n* does not describe the number of sites per particle *N*: indeed, a macromolecule with *N* identical, independent sites (Langmuir model) will always show a Hill plot with *n*=1.

We return to approaches for describing ligand interactions on NCs below, but first, we will look at extensions to the case of independent (non-interacting) sites.

4.2 Ligand exchange reactions and Langmuir-like limits

In many cases, NC surface chemistry entails ligand exchange, not ligand association to vacant (solvent-occupied) sites. Ligand exchange, in which a pre-existing ligand is displaced, can be modeled thermodynamically as competitive binding of pre-existing (native) and new ligands to sites on the NC surface (Figure 9B). In the case of identical independent sites, the most general solution requires simultaneous equilibrium of the chemical equations for binding of each ligand to vacant sites S:

$$\mathbf{S} + \mathbf{L_1} = \mathbf{SL_1} \quad (6a)$$

$$\mathbf{S} + \mathbf{L_2} = \mathbf{SL_2} \quad (6b)$$

where L_1 is the initial ligand, L_2 is the new ligand, and SL_1 and SL_2 respectively represent sites occupied by each, with the corresponding mass action expressions for the association constants $K_{a,L1}$ and $K_{a,L2}$ for each ligand, where ϑ_1 and ϑ_2 represent the fractional occupancy of sites by L_1 and L_2 respectively:

$$\boldsymbol{K_{a,L1}} = \frac{[\mathbf{SL_1}]}{[\mathbf{S}]}\frac{\mathbf{1}}{[\mathbf{L_1}]} = \frac{\boldsymbol{\theta_1}}{(\mathbf{1}-\boldsymbol{\theta_1}-\boldsymbol{\theta_2})[\mathbf{L_1}]} \quad (7a)$$

$$\boldsymbol{K_{a,L2}} = \frac{[\mathbf{SL_2}]}{[\mathbf{S}]}\frac{\mathbf{1}}{[\mathbf{L_2}]} = \frac{\boldsymbol{\theta_2}}{(\mathbf{1}-\boldsymbol{\theta_1}-\boldsymbol{\theta_2})[\mathbf{L_2}]} \quad (7b)$$

With the number of sites and association constants as parameters, these linked quadratic equations can be solved for $[L_2]$, and used to determine the amount of each ligand bound for any combination $[M]_t$, $[L_1]_t$, and $[L_2]_t$.

Competitive binding is routinely encountered in biochemistry and catalysis, and programs to fit analytical results, such as ITC, in terms of a competitive binding model are routinely available. However, it may not be possible, or necessary, to resolve the complete parameter set ($K_{a,L1}$, $K_{a,L2}$, N, plus ΔH_{L1} and ΔH_{L2} for ITC) to describe the results for a particular experiment. A common situation for NCs is that that surface is initially saturated with one ligand so that there are very few vacant sites throughout the course of the experiment. In this case, binding of one ligand always requires displacement of the other, and the two equilibria can be collapsed to a single expression defining the exchange equilibrium constant K_{ex}:

$$\mathbf{SL_1} + \mathbf{L_2} = \mathbf{SL_2} + \mathbf{L_1} \quad (8a)$$

$$\boldsymbol{K_{ex}} = \frac{\boldsymbol{K_{a,L2}}}{\boldsymbol{K_{a,L1}}} = \frac{\boldsymbol{\theta_2}[\mathbf{L_1}]}{(\mathbf{1}-\boldsymbol{\theta_2})[\mathbf{L_2}]} \quad (8b)$$

Where ϑ_2 is the fractional occupation of sites by the new ligand L_2. The condition at equilibrium can be solved exactly when the total concentrations of ligands and macromolecule are known, for any set of N and K_{ex}. ITC will also obtain the difference in enthalpy of binding ΔH_{ex} between L_1 and L_2, reducing the parameter set to 3 from 5 for the general case. However, in general we do not know what will be an appropriate thermodynamic model for a reaction before we conduct an experiment, and so it is helpful to examine the behavior of the 1:1 ligand exchange model in several limits.

The simplest limit mathematically is saturating conditions, in which the concentration of L_1 in solution is much greater than the total concentration of sites ($[L_1] \gg N[M]_t$) so that displacement of L_1 from the surface makes a negligible change in $[L_1]$ over the course of the reaction, so that $[L_1]$ can be considered constant. In this case, we can define an effective association constant $K_{a,eff}$ for new ligand L_2 that applies at this particular concentration of $[L_1]$:

$$\frac{\boldsymbol{\theta_2}}{(\mathbf{1}-\boldsymbol{\theta_2})[\mathbf{L_2}]} \approx \boldsymbol{K_{a,eff}} = \frac{\boldsymbol{K_{ex}}}{[\mathbf{L_1}]} \quad (9)$$

A Langmuir-like mass action expression is recovered; experimental data can be fit in terms of the Langmuir model to arrive at $K_{a,eff}$, and with knowledge of $[L_1]$, the exchange equilibrium constant K_{ex} can be obtained. This technique is somewhat unwieldy in that it requires a large excess concentration of the initial ligand, which tends to suppress ligand exchange; only for sufficiently large values of K_{ex} and $[M]_t$, such that $c=K_{a,eff}N[M]_t \gg 1$, can the number of sites N be obtained with precision from ITC alone. However, saturating conditions can be useful in providing colloidal stability when using a weakly associating initial ligand L_1 as a "leaving group" for installation of several stronger binders L_2, for which K_{ex} and ΔH can be compared from parallel titrations.[56]

The more common case for NC ligand exchange is that the sites are nearly filled with the initial ligand L_1, but the concentration of L_1 in solution is low, such that $[L_1]_t$ is approximated by the total concentration of sites ($[L_1]_t \approx N[M]_t$). This is typically the case for quantum dots with anionic organic ligands following initial purification in nonpolar solvents, for example.[60,170,214] In such cases, the primary source of L_1 in solution will be displacement by binding of new ligand L to some of the sites on the NC surface: $[L_1] \approx \vartheta_2 N[M]_t$. Unlike in the saturation limit, $[L_1]$ changes by a large factor as L_2 is introduced. However, with $K_{ex} \gg 1$, the dependence of ϑ_2 (or measured heat in ITC) on $[L_2]_t$ once again resembles a Langmuir-Weissman isotherm. This is because the system only deviates from quantitative exchange near the equivalence point where $[L_2]_t \approx N[M]_t$. Here, ϑ_2 is approaching 1, and so $[L_1] \approx N[M]_t$, giving an effective association constant $K_{a,eff}=K_{ex}/(N[M]_t)$. Hence, analyzing isotherms from such an experiment in terms of the Langmuir model will give $K_{a,eff}$, N, and ΔH_{ex}, and N and $[M]_t$ can be used to obtain K_{ex}. The exact solution to Equation 8b closely resembles this limit for $K_{ex} \geq 5$.[59]

Exchange at identical independent sites has been relatively successful at describing X-type anionic exchange of alkylcarboxylate with thiols on CdSe[60] and PbS[147] NCs and InP

clusters[157] in anhydrous solvents, though deviations appear under some conditions as described below. It has been less successful at describing exchange of alkylcarboxylates with phosphonic acids,[59,62,157] where deviations from the Langmuir-like limits described above appear. At least in the case of InP, it appears this may be partly corrected by considering 2-for-1 exchange due to the diprotic character of phosphonic acids.[157] Likewise, Jharimune *et al.* observed excellent compliance with the Langmuir limit for bulk cation exchange of Cd^{2+} in CdSe NCs with 2 equivalents of Ag^{+}.[65] While not strictly a ligand exchange reaction, they were able to resolve variation in the ion exchange enthalpy and entropy among different ligand coatings on the NCs (**Figure 11**).

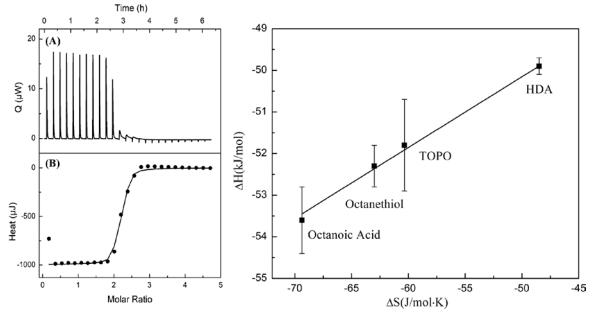

Figure 11. Left, thermogram and isotherm for ion exchange of CdSe NCs to yield Ag_2Se. The first titration point is neglected as is conventional due to pre-mixing. Right, ΔH and ΔS for ion exchange in the presence of several surface ligands. Adapted with permission from Jharimune *et al.*, Ref. 65. Copyright 2018 American Chemical Society.

4.3 Multiple types of independent sites

The surfaces of NCs are intrinsically heterogeneous due to the presence of facets (often several types), edges, corners, and various defects and reconstructions. In some cases it is possible to resolve ligand populations in different surface environments spectroscopically, for example by shifts in NMR or IR spectra. It may also be possible to resolve different types of binding sites thermodynamically. In principle, one set of sites could react completely with an added ligand under conditions where other sites react negligibly; in this case, the Langmuir assumption of identical sites might hold for describing those sites that do react. However, in other cases, multiple sets of sites may be able to undergo reactions at experimentally accessible reagent concentrations, but with different equilibrium constants. In this case, the extent of reaction (fractional occupation, for ligand binding or exchange) at multiple sets of sites must simultaneously reach equilibrium with reactant concentrations in solution, and we may be interested in understanding whether it is possible to selectively modify one set, or whether observed spectroscopic or ITC data can be explained in terms of reactions at several types of sites, each with a unique set of thermodynamic parameters. As in the case of identical sites, the simplest model considers independent sites (Figure 9C).

Consider binding of a ligand L to two types of initially vacant, independent sites with association constants K_{a1} and K_{a2}:

$$\boldsymbol{K_{a1}} = \frac{\boldsymbol{\theta_1}}{\boldsymbol{(1-\theta_1)[L]}} \qquad (10a)$$

$$\boldsymbol{K_{a2}} = \frac{\boldsymbol{\theta_2}}{\boldsymbol{(1-\theta_2)[L]}} \qquad (10b)$$

These linked equations can be solved exactly (now requiring a cubic polynomial) to determine the isotherm for any set of the 6 parameters K_{a1}, K_{a2}, ΔH_1, ΔH_2, N_1, and N_2 where N_1 and N_2 are the number of sites of each type per macromolecule. Ligand L will tend to bind first to the sites with the largest K_a. A particular advantage of ITC is that it can distinguish binding to different types of sites based on differences in ΔH;[48,49] this can enable the populations of different types of sites to be resolved and compared to structural measurements. In contrast, NMR may be limited to measuring the total populations of bound and free ligands, which can be hampered by very low free ligand concentrations. Talapin has compared electrochemical measurements of free ligand concentration (which depend on log [L]) to NMR and shown that, if the different bound forms cannot be resolved, NMR is limited to resolving sites with $K_{a1}/K_{a2} \geq 10^6$ while electrochemical methods can get to $\geq 10^4$.[215] We have pointed out[59,141] that ITC can resolve sites with $K_{a1}/K_{a2} > 10^2$ as long as ΔH_1 and ΔH_2 are significantly different. ITC analysis software is routinely equipped to fit data in terms of association to two or three types of independent sites; Rioux has applied this analysis to thiol association to Au NCs.[64]

Models for exchange at multiple types of sites (in which sites may be initially occupied) involve a similar parameter set but will generally require use of effective association constants as in section 4.3 and/or customized analytical solutions; symbolic math software can assist in solving for [L] in terms of $[L]_t$, $[M]_t$, and initial ligand concentration(s) in these cases. We found evidence via ITC that phosphonic acids can bind to ZB CdSe NCs with initial oleate X-type ligand coordination both through X-type exchange of oleate, and through adsorption of the neutral compound to vacant sites.[59] Similar behavior has been reported for carboxylic and phosphonic acids on InP clusters, in contrast to the case for thiol addition where X-type exchange predominated.[157] Banin's group has found that isotherms for titration of oleate-capped ZB CdSe with thiols reveal multiple types of X-type exchange sites in the case of short, linear alkane tails.[60] Examination of a family of branched and linear tails showed the branched ones could maintain high K_a, despite being less exothermic, due to a smaller entropic penalty on binding, as well as evidence for sites with different steric constraints (**Figure 12**).[61] NMR studies of displacement of $Cd(oleate)_2$ (Z-type ligands) from ZB CdSe NCs[216] and $Pb(oleate)_2$

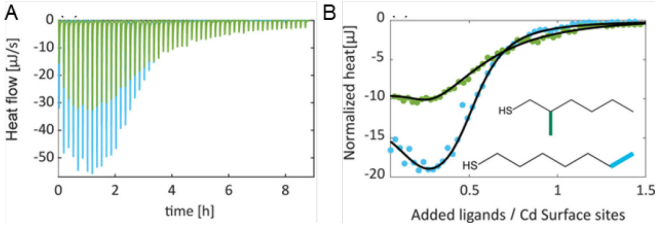

Figure 12. Thermograms (A) and isotherms (B) for exchange of oleate with linear and branched thiols on ZB CdSe NCs. The curves represent exchange at two sets of independent sites and in this case, the sites with the largest K_{ex} have the less negative enthalpy change. Adapted with permission from Elimelech *et al.*, Ref. 61 (CC-BY-4.0).

from rocksalt PbS NCs[140] by high concentrations of amine nucleophiles have also been interpreted in terms of two sets of sites. In the latter case, the site numbers for weaker binders could be indexed to corners on an octahedral structural model for the NC.

4.4 Fowler adsorption isotherm

Interactions among molecules at nearby binding sites are known to strongly influence the growth of crystals[142,217] and the thermodynamics of self-assembled monolayers;[218] they also play a prominent role in NC surface chemistry. The influence of interactions can be seen, for instance, in ligand densities for nucleophiles with different steric requirements on NCs in non-polar solvents,[219,220] and in the relative stability of NCs protected by small molecule ligands with longer alkyl linkers in aqueous solution.[221]

From the perspective of thermodynamic models, the question is whether such interactions can be interpreted simply in terms of corrections to the parameter set for independent binding, or whether interactions must be considered explicitly. Even in the former case, examining models that incorporate interactions could help to understand how the empirical thermodynamic parameters obtained from experiments may differ from those predicted from simple structural models.

One of the simplest approaches to treating interactions is the Fowler adsorption isotherm,[222] summarized in Figure 9D, in which an interaction term is added to the free energy of the system that depends linearly on the fractional occupation ϑ. An interaction parameter W is defined, representing a sum of pairwise interactions experienced by each ligand, such that the average interaction free energy per site is $W/2$ as ϑ approaches 1. The mass action expression becomes:

$$\boldsymbol{K}_{\mathbf{a}} = \frac{\boldsymbol{\theta}}{(\mathbf{1}-\boldsymbol{\theta})[\mathbf{L}]} \boldsymbol{e}^{\frac{\boldsymbol{2W}}{\boldsymbol{RT}}\boldsymbol{\theta}} \qquad (11)$$

with $W<0$ representing cooperative interactions such that the association constant appears to increase with ϑ, and $W>0$ the opposite. A linearized plot may be obtained by plotting $\ln([L](1-\vartheta)/\vartheta)$ versus ϑ:

$$\boldsymbol{ln}\left([\mathbf{L}]\frac{\mathbf{1}-\boldsymbol{\theta}}{\boldsymbol{\theta}}\right) = -\boldsymbol{ln}\,\boldsymbol{K}_{\mathbf{a}} + \frac{\boldsymbol{2W}}{\boldsymbol{RT}}\boldsymbol{\theta} = \frac{\boldsymbol{\Delta G}}{\boldsymbol{RT}} + \frac{\boldsymbol{2W}}{\boldsymbol{RT}}\boldsymbol{\theta} \qquad (12)$$

We see that K_a and ΔG in the above expression are those that would describe the Langmuir model in the limit of low ϑ. This model was used by Quarta *et al*. to infer anti-cooperative interactions between sterically bulky ammonium ligands on halide perovskite NCs, while primary ammonium ligands showed cooperative interactions, with turbidity used as a proxy for ligand binding.[223] Interestingly, *cooperative* interactions were reported earlier by Moreels *et al.* for TOP/TOPO ligands on InP NCs;[54] the difference might be related to particle size or shape, with the InP NCs having a smaller radius permitting a greater cone angle for bound ligands. Kroupa *et al.* used the Fowler isotherm to describe ligand exchange of cinnamic acids onto oleate-capped PbS QDs and observed strongly cooperative behavior with $2W \approx -15$ kJ/mol.[224] Such cooperativity could help to explain the success of fluorocinnamic acids in preparation of stable PbS and $AgBiS_2$ NC inks.[158] A limitation of the Fowler model is that it only considers association of a single type of ligand and the value of the interaction free energy obtained may be difficult to compare directly to computational results or structure-based estimates of ligand size. We are unaware of examples of the Fowler isotherm applied to NC ITC studies, but note that isotherms would be sensitive to entropic and enthalpic contributions to W.

4.5 McGhee-von Hippel adsorption isotherm

A step beyond mean-field approaches to ligand interactions are lattice models, in which ligands bind to a 1-dimensional (1D) or 2D lattice of possible binding sites.[222] The 1D lattice model has been applied to binding of ligands to biopolymers such as nucleic acids. An important feature is the ability to consider steric effects that arise when binding of a large ligand occupies several contiguous binding sites. At low occupancy, there are many possible locations such a ligand can bind; at high occupancy, even if some sites are vacant, it is less probable that contiguous sites are available that can accommodate the "footprint" of the bulky ligand. The McGhee-von Hippel formalism[45,225] gives closed-form solutions to binding of ligands with footprint length l sites to a 1D lattice. For length $l>1$, an anti-cooperative effect (compared to a Langmuir model with the same maximum number N of ligands at saturation) is observed simply from the combinatorial (entropic) effect of requiring contiguous sites for binding (Figure 9E). This can be seen by adapting the notation used in Brown's review,[45] which derives from Scatchard analysis in molecular biology, to that of the present article. Letting N_s represent the number of lattice sites, with N continuing to represent the maximum possible number of ligands bound per macromolecule so that $N \approx N_s/l$, and allowing ϑ_L to represent the average number of ligands bound as a fraction of N ($\vartheta_L=[L]_b/(N[M]_t)$), and solving for the association constant K_a for binding of a ligand to the lattice in the limit of low occupancy, we can write:

$$K_{\mathrm{a}} = \frac{\theta_{\mathrm{L}}}{l(1-\theta_{\mathrm{L}})^{l}[\mathrm{L}]}\left[1-\theta_{\mathrm{L}}\left(\frac{l-1}{l}\right)\right]^{l-1} \qquad (13)$$

It can be seen that this reduces to the Langmuir model for $l=1$. Additional parameters for nearest-neighbour cooperativity and enthalpy corrections can be included.[45] Ligand densities at NC surfaces are known to frequently be below the density of possible coordination sites as dictated by the crystal lattice.[61,134,138,149,219,226] Many studies have used 2D or 3D lattice models to enable statistical consideration of steric and solvation effects in the binding of polymer chains to surfaces.[133] In addition to considering homogeneous or inhomogeneous[227] planar surfaces, these expand on the conformations enumerated in the McGhee-von Hippel model by considering polymer segments as "trains" (occupying consecutive nearest-neighbour sites), "loops" (unbound segments between trains), and "tails" (unbound ends). Such approaches these are likely to be relevant to consideration of polymer ligand coordination of NCs[134] but we are unaware of examples that implement such models for quantitative interpretation of ITC data or NC-ligand binding equilibria.

4.6 Lattice simulations

An alternative approach to lattice-based models of ligand binding to NC surfaces is simulations that simply add up ligand-surface and nearest-neighbour interactions for representative surface configurations (Figure 9F). Configurations can be permuted or evaluated in a Monte-Carlo fashion to learn the characteristics of the ensemble when the free energy is minimized at a given temperature.[228] This approach has recently been used by the Alivisatos group to analyze deviations from the Langmuir model identified from correlated NMR and ITC measurements in several types of small molecule ligand-NC binding interactions.[62,63] Advantages include the ability to consider 2D surfaces, interactions among multiple ligand types as encountered in ligand exchange reactions, phase separation, and the possibility of vacant sites. A 2D "Ising model" considers only that nearest-neighbour sites be occupied, or not occupied, by the ligand being introduced: it can consider association to a vacant surface, or strict exchange, as a function of free ligand concentration; nearest-neighbour terms are notated as "tail" parameters. A modified Ising model was applied to consider exchange in the presence of vacant sites, in which case terms for same (A-A,B-B) and different (A-B) interactions must be included. These models can account for many features of experimentally observed isotherms (**Figure 13**). Challenges include the large parameter set, particularly for exchange and association, that places high demands on experimental data to obtain unique solutions. A useful innovation in these papers is using the NMR measurements of surface occupancy to produce plots of the incremental enthalpy per mole ligand added to the surface, rather than incremental enthalpy per mole ligand added to the system as a whole.

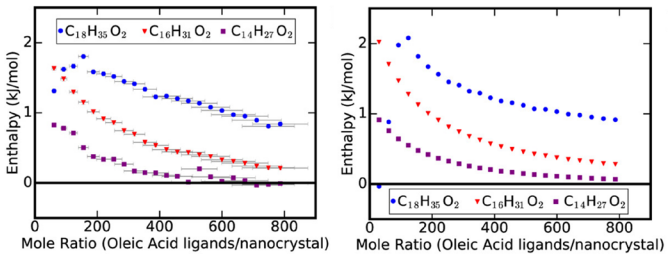

Figure 13. Isotherms (left, experimental: right, calculated via modified Ising lattice model) for titration of several saturated alkylcarboxylic acids into oleate-capped InP NCs in toluene. Here, the vertical axis represents the measured heat per injection (from ITC) divided by the change in the moles of bound ligand (from NMR). Adapted with permission from Calvin *et al.*, Ref. 62. Copyright 2021 American Chemical Society.

5. Reconciling with structural models

5.1 Solid State NMR

While transmission electron microscopy and X-ray diffraction are useful in probing the core structure of NCs, solid-state NMR (SSNMR) is beneficial in acquiring structural information of the bound ligands and providing information about the heterogeneity of the NC surfaces. Conventional nuclei found in NCs like ^{29}Si, ^{31}P, ^{77}Se, ^{113}Cd, ^{123}Te, ^{133}Cs, and ^{207}Pb show narrow SSNMR signals assigned to the core atoms of the NCs however the surface atoms of a similar diameter NC may show broadened and shifted SSNMR signals.

Cross-polarization magic angle spinning (CP-MAS) SSNMR spectroscopy technique has been identified in numerous applications in characterizing the surface selective structures of NCs. For example, ^{1}H → ^{77}Se CP and CP-heteronuclear correlation (CP-HETCOR) experiments on CdSe NCs showed distinctive surface ^{77}Se chemical shifts compared to the core Se atoms confirming that surface Se atoms have unique structural parameters and chemical environments that deviate from their bulk counterparts.[229,230] Recent work from Rossini and coworkers has shown advancement of the field by utilizing dynamic nuclear polarization (DNP) enhanced ^{77}Se and ^{113}Cd SSNMR to further reveal the surface structure of the CdSe nanoplatelets and nanospheroids.[231] They found that the surfaces of both CdSe nanoplatelets and nanospheroids primarily consist of {100} Se surfaces [$Se(Cd_{core})_2(Cd_{surface})_2$ units], where the cadmium atoms at the surface comprise $Cd(Se_{surface})_2(O_2CR)$ units. CsBr termination of the $CsPbBr_3$ NCs was identified by Rossini and Brutchey applying SSNMR spectroscopy.[87] Fast magic angle spinning (MAS) SSNMR has been used to enhance the surface selectivity where ^{133}Cs spectra show the presence of an additional ^{133}Cs NMR signal, indicating the NC surface is terminated with Cs ions. Further, ^{1}H–^{133}Cs and ^{1}H–^{207}Pb internuclear distance measurements between dodecylammonium–NH_3^+ ligand protons and surface and subsurface ^{133}Cs and ^{207}Pb spins indicate that the CsBr is interacting with alkylammonium ligands on a particular surface site.

5.2 Computational models

The complex nature of NC surfaces makes them challenging to study experimentally, and also an interesting computational challenge. Density functional theory (DFT) calculations have emerged as the primary techniques to predict structure at the NC-ligand interface and to link such structures to NC optoelectronic properties, while atomistic molecular dynamics calculations provide a view into inter-ligand and ligand-solvent interactions.[52,113,217,232–239]

To simplify the NC system and reduce the computational cost, often clusters or smaller size NCs have been used for DFT calculations. In 2011, Voznyy provided the first atomistic model to explain the emission wavelength and lifetime variations, and blinking of the NCs using realistic CdSe NCs with carboxylic acid ligands (**Figure 14**).[232] He showed it is possible to construct NCs without electronic traps even in the presence of surface atoms with dangling bonds. Extending this lead, Infante and coworkers

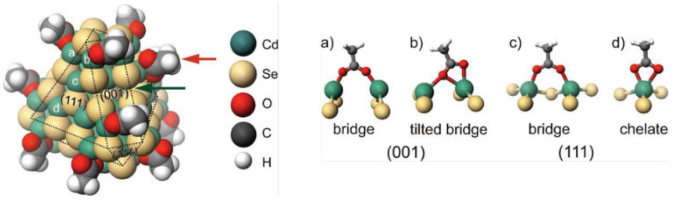

Figure 14. Left, optimized structure of a $[Cd_{56}Se_{50}(OAc)_{13}]^{1-}$ NC used in calculations by Voznyy. Right, optimized geometries of acetate on CdSe NC surface: a,b on (001) Cd-rich surface facet: c,d on (111) Cd-rich facet. Adapted with permission from Ref. 232, published 2011 American Chemical Society.

studied ligand surface coordination in terms of L-, X-, and Z-type ligands; they showed that most under-coordinated "dangling" atoms do not form traps and that L- and X-type ligands are gentle to the NC structure.[238] Also, they found clear evidence that Z-type displacement generates midgap states, localized on the 4p lone pair of 2-coordinated selenium surface atoms in ZB II–VI metal chalcogenide NCs of any size and shape.

6. Thermodynamics as a guide for future development of NC coordination

A deeper understanding of thermodynamic parameters in NCs can resolve trade-offs in design where variation in ligand concentration can result in either beneficial surface passivation or detrimental etching.[57,89,216] It can also streamline the choice of polymer binding motifs and architecture for the creation of highly stable water soluble NCs, as discussed in Section 2. Thermodynamic studies can also lead to superior regioselective control of NC surface chemistry. We consider a few of these possibilities below.

6.1 Optimizing ligand coverage for stable perovskite NCs

Thermodynamic investigations can help navigate gaps in the understanding of various NC-ligand systems. For example, we were inspired by apparent discrepancies regarding the stabilization of $CsPbBr_3$ NCs through surface modification with dimethyldidodecyl ammonium bromide (DDAB). Some researchers reported the occurrence of a phase transformation into two-dimensional (2D) $CsPb_2Br_5$ nanoplatelets[240] upon DDAB treatment while others reported improved quantum yield and stability.[88,102] Through ^{1}H NMR titration, ITC, and TEM, we were able to distinguish two key processes that occur during the NC-ligand exchange with DDAB.[57] The first step of the process is endothermic and involves the dual exchange of oleate and oleylammonium with DDA+/Br- on the NC surface. As the first step approaches completion, a second step commences where Pb-containing complexes are displaced. This step is exothermic and initiates a third, more slowly-proceeding step involving Ostwald ripening of the NCs due to the Pb-containing complexes in solution. Arresting the exchange at the conclusion of the first step enables isolation of highly stable, DDAB-capped $CsPbBr_3$ NCs.[89] The sensitivity of ITC to ΔH allowed the processes to be distinguished clearly (**Figure 15**), while ^{1}H NMR helped to identify the products.

6.2 Polymer ligands: optimizing stability, surface protection, and interactions with different NC surfaces

While the high stability of semiconductor NCs coated with multiply-binding polymers compared to small molecules with similar binding motifs has been noted,[135] there remains interest in how the architecture, for example the monodentate or bidentate binding motifs[241] and the sequence of binding vs. stabilizing monomer residues in polymeric ligands, influences colloidal stability and protection of the surface against undesired interactions with endogenous molecules in biological systems. In our comparison of block- and random-copolymer methacrylate-based polymeric imidazole ligands, CdSe/CdZnS

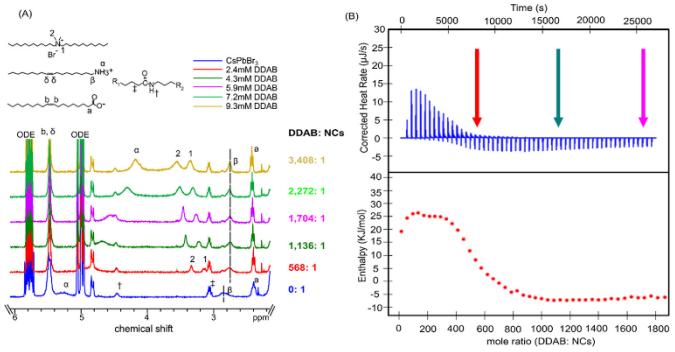

Figure 15. A, NMR titration and B, ITC titration of DDAB into $CsPbBr_3$ NCs with native oleate/oleylammonium ligands. Arrows indicate points equivalent to first 3 NMR titration points. Adapted with permission from Abiodun *et al.* Ref. 57. Copyright 2021 American Chemical Society.

NCs exchanged with polymers were titrated with L-glutathione (an intracellular antioxidant) at physiological pH. Stability of the NCs was assessed by PL changes;[106] it was found that NCs coated with block copolymers were least susceptible to glutathione association and were overall more stable than random copolymer NCs. Multiply-binding block copolymers are also of interest for magnetic oxide NCs[242] and more detailed thermodynamic investigation could aid in development of improved bioimaging probes.

6.3 Regioselective surface chemistry

Progress in the understanding of thermodynamic parameters of NC surface chemistry would also permit regioselective control over the NC surface. As noted by Hoang *et al.*, currently, it is very challenging to accurately determine ligand shell structure on NC surfaces, though NMR and scanning electron energy loss spectroscopy (EELS) have shown great potential.[43] Combining ITC with such spectroscopic and structural analyses could help separate the role of entropy and enthalpy in determining phase separation and formation of locally-ordered phases on NC surfaces, aiding in rational design of NC surfaces for various applications. For example, NCs have found use as fluorescent probes in neuroscience applications;[14,243] one goal in this field is to develop cell membrane-targeted voltage sensors that provide the fastest response time and best optical resolution for imaging the propagation of action potentials. In 2013, Marshall and Schnitzer proposed the use of NCs as voltage sensors that would out-perform standard biological voltage sensors in their response speed, size, and voltage-dependent optical properties (**Figure 16**).[244] They outlined two ways in which NCs could function as voltage sensors: one where the NCs are coated uniformly with hydrophobic surface molecules and are embedded within the cell membrane,[245] and another where the NCs have distinct hydrophobic and hydrophilic surface regions so that they can be implemented as transmembrane molecules. In order to efficiently and successfully produce these NC voltage sensors, a strong foundation of NC surface thermodynamics would need to be established and this could be completed with the aid of ITC experimentation to resolve, for example, sites on the hexagonal axes and orthogonal sidewalls of wurtzite NCs.[246]

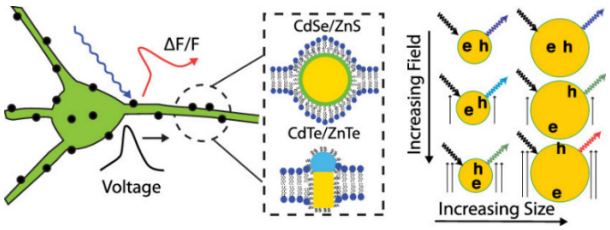

Figure 16: Concept for membrane-embedded NC voltage sensors envisioned by Marshall and Schnitzer. Reprinted with permission from Ref. 244. Copyright 2013 American Chemical Society.

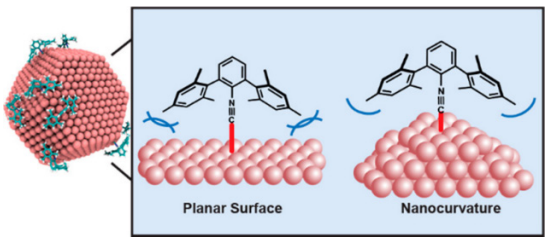

Figure 17: Sterically-shielded isocyanide ligand selectively coordinates sites of high local curvature on Au NCs. Reprinted with permission from Wang *et al*., Ref. 220. Copyright 2022 American Chemical Society.

A recent step toward regioselective control of NC surfaces has been made by Wang *et al.* involving *m*-terphenyl isocyanide ligands on Au NCs (**Figure 17**).[220] It was shown, both experimentally and computationally, that the steric interference between the anchoring group of the ligands and the surface of the NC was the dominating force driving the ligand's affinity for the curved edges of the NC rather than the planar facets. This research further emphasizes the role of ligand design, including entropic contributions to thermodynamics that are challenging to model computationally, in enabling advanced control of NC-based structures. It could be an exciting system to study with ITC.

6.4 Translation of thermodynamic understanding across various nanocrystalline chemistries

While this Article has focused heavily on chalcogenide, pnictide, and perovskite semiconductor NCs, NC-ligand interactions are important to the function of many other types of inorganic nanoparticles (NPs) including metals and metal oxides that comprise a major portion of inorganic NPs successfully adapted for clinical use. These can be evaluated with similar techniques, but will display very different chemistry, from the semiconductor NCs described above. Extensive investigation into surface modification techniques and subsequent colloidal stability of metal and metal oxide NPs has been carried out, largely in aqueous environments. Using ITC, early work in the area by Chiad *et al*. demonstrated how quantitative binding profiles of polymer interactions with SiO_2 NPs could be established, resulting in a highly informative profile that can be used to optimize the surface chemistry of SiO_2 for various applications.[247] Additionally, magnetic iron oxide (Fe_3O_4) nanoparticles have seen major developments over the last few decades as magnetic tracers in bioimaging, biosensing, and drug delivery. A large variety of modification procedures have been applied to these metal oxide surfaces, supporting a number of ligand architectures similar to those previously discussed with metal-chalcogenide NCs.[242] While Rioux's group has used ITC to directly study thiol coordination of Au NPs, functionalized Au NPs have also been employed to study the influence of coatings on non-specific binding,[248,249] and as a platform to study specific biomolecular and biomimetic interactions via ITC.[250–252]

7. Conclusions

Merely a decade ago, there were only a very few examples of NC-ligand thermodynamic measurements,[54] or stoichiometric ligand exchange reactions of any kind on semiconductor NCs in solution,[163] despite striking demonstrations of the unique physical properties of NCs and the beginning of commercial applications of quantum dots. Yet, the groundwork had been laid by development of syntheses for NCs and clusters with low dispersity, identification and classification of some of the most important binding motifs for organic ligands on NC surfaces,[253] and development of atomistic computational models that include surface coordination.[232] In the time since, there have been very rapid advances in knowledge fueled by new reactions, purification techniques, measurement techniques, and modeling approaches. One of the most important aspects has been the development an NMR "toolbox" that has been widely adopted.[166] Wielding an ever greater set of tools, including ITC, will lead to even greater capabilities to learn and innovate with NC surface chemistry.

Author Contributions

All authors have contributed to writing and editing of this Feature Article.

Conflicts of interest

There are no conflicts to declare.

Acknowledgements

We acknowledge research support from the US National Science Foundation under grant numbers CHE-1613388 and CHE-2109064, with additional support from MADE in SC under NSF OIA-1655740. Support from the University of South Carolina including the ASPIRE program is also acknowledged. We thank Dr. Caryn Outten for helpful discussions, and Dr. Corey Martin for a critical reading of the manuscript.

Notes and references

1 J. Owen, *Science*, 2015, **347**, 615–616.

2 C. J. Murphy and J. M. Buriak, *Chem. Mater.*, 2015, **27**, 4911–4913.
3 J. S. Beveridge, M. R. Buck, J. F. Bondi, R. Misra, P. Schiffer, R. E. Schaak and M. E. Williams, *Angew. Chem. Int. Ed.*, 2011, **50**, 9875–9879.
4 M. Green, *J. Mater. Chem.*, 2010, **20**, 5797–5809.
5 M. Noh, T. Kim, H. Lee, C.-K. Kim, S.-W. Joo and K. Lee, *Colloids and Surfaces A: Physicochemical and Engineering Aspects*, 2010, **359**, 39–44.
6 W. R. Algar, M. Massey, K. Rees, R. Higgins, K. D. Krause, G. H. Darwish, W. J. Peveler, Z. Xiao, H.-Y. Tsai, R. Gupta, K. Lix, M. V. Tran and H. Kim, *Chem. Rev.*, 2021, **121**, 9243–9358.
7 E. N. Bodunov and A. L. Simões Gamboa, *J. Phys. Chem. C*, 2019, **123**, 25515–25523.
8 M. Kuno, J. K. Lee, B. O. Dabbousi, F. V. Mikulec and M. G. Bawendi, *Journal of Chemical Physics*, 1997, **106**, 9869–9882.
9 B. R. Fisher, H. J. Eisler, N. E. Stott and M. G. Bawendi, *Journal of Physical Chemistry B*, 2004, **108**, 143–148.
10 F. Ahmed, J. H. Dunlap, P. J. Pellechia and A. B. Greytak, *Chem. Commun.*, 2021, **57**, 8091–8094.
11 A. Heuer-Jungemann, N. Feliu, I. Bakaimi, M. Hamaly, A. Alkilany, I. Chakraborty, A. Masood, M. F. Casula, A. Kostopoulou, E. Oh, K. Susumu, M. H. Stewart, I. L. Medintz, E. Stratakis, W. J. Parak and A. G. Kanaras, *Chem. Rev.*, 2019, **119**, 4819–4880.
12 J. Chang and E. R. Waclawik, *RSC Advances*, 2014, **4**, 23505–23527.
13 M. Liu, N. Yazdani, M. Yarema, M. Jansen, V. Wood and E. H. Sargent, *Nat Electron*, 2021, 1–11.
14 S. J. Lim, L. Ma, A. Schleife and A. M. Smith, *Coordination Chemistry Reviews*, 2016, **320–321**, 216–237.
15 J. T. DuBose and P. V. Kamat, *J. Phys. Chem. Lett.*, 2019, **10**, 6074–6080.
16 J. T. DuBose and P. V. Kamat, *ACS Energy Lett.*, 2022, **7**, 1994–2011.
17 E. A. Weiss, *ACS Energy Lett.*, 2017, **2**, 1005–1013.
18 Z. Huang and M. L. Tang, *J. Phys. Chem. Lett.*, 2018, **9**, 6198–6206.
19 L. Nienhaus, M. Wu, V. Bulovic, M. A. Baldo and M. G. Bawendi, *Dalton Trans.*, 2018, **47**, 8509–8516.
20 I. L. Medintz, H. T. Uyeda, E. R. Goldman and H. Mattoussi, *Nat Mater*, 2005, **4**, 435–446.
21 P. R. Brown, D. Kim, R. R. Lunt, N. Zhao, M. G. Bawendi, J. C. Grossman and V. Bulović, *ACS Nano*, 2014, **8**, 5863–5872.
22 E. C. Hansen, Y. Liu, H. Utzat, S. N. Bertram, J. C. Grossman and M. G. Bawendi, *Angewandte Chemie International Edition*, 2020, **59**, 860–867.
23 P. D. Howes, R. Chandrawati and M. M. Stevens, *Science*, 2014, **346**, 1247390.
24 A. M. Wagner, J. M. Knipe, G. Orive and N. A. Peppas, *Acta Biomaterialia*, 2019, **94**, 44–63.
25 X. Wu, H. Liu, J. Liu, K. N. Haley, J. A. Treadway, J. P. Larson, N. Ge, F. Peale and M. P. Bruchez, *Nat Biotech*, 2003, **21**, 41–46.
26 J. De Roo, I. Van Driessche, J. C. Martins and Z. Hens, *Nat Mater*, 2016, **15**, 517–521.
27 J. De Roo, Y. Justo, K. De Keukeleere, F. Van den Broeck, J. C. Martins, I. Van Driessche and Z. Hens, *Angewandte Chemie International Edition*, 2015, **54**, 6488–6491.
28 L. Du, W. Wang, C. Zhang, Z. Jin, G. Palui and H. Mattoussi, *Chem. Mater.*, 2018, **30**, 7269–7279.
29 L. Deblock, E. Goossens, R. Pokratath, K. De Buysser and J. De Roo, *JACS Au*, 2022, **2**, 711–722.
30 M. A. White, J. A. Johnson, J. T. Koberstein and N. J. Turro, *J. Am. Chem. Soc.*, 2006, **128**, 11356–11357.
31 A. M. Alkilany, S. R. Abulateefeh, K. K. Mills, A. I. Bani Yaseen, M. A. Hamaly, H. S. Alkhatib, K. M. Aiedeh and J. W. Stone, *Langmuir*, 2014, **30**, 13799–13808.
32 N. A. Nosratabad, Z. Jin, L. Du, M. Thakur and H. Mattoussi, *Chem. Mater.*, 2021, **33**, 921–933.
33 S. F. Sweeney, G. H. Woehrle and J. E. Hutchison, *J. Am. Chem. Soc.*, 2006, **128**, 3190–3197.
34 N. Alele, R. Streubel, L. Gamrad, S. Barcikowski and M. Ulbricht, *Separation and Purification Technology*, 2016, **157**, 120–130.
35 G. Chen, Y. Wang, L. H. Tan, M. Yang, L. S. Tan, Y. Chen and H. Chen, *J. Am. Chem. Soc.*, 2009, **131**, 4218–4219.
36 D. Zhang, X. Ma, Y. Gu, H. Huang and G. Zhang, *Frontiers in Chemistry*, 2020, **8**, 799.
37 G. Habibullah, J. Viktorova and T. Ruml, *Nanoscale Research Letters*, 2021, **16**, 47.
38 M.-C. Daniel and D. Astruc, *Chem. Rev.*, 2004, **104**, 293–346.
39 K. L. Kelly, E. Coronado, L. L. Zhao and G. C. Schatz, *J. Phys. Chem. B*, 2003, **107**, 668–677.
40 Y. G. Sun and Y. N. Xia, *Science*, 2002, **298**, 2176–2179.
41 X. Huang, I. H. El-Sayed, W. Qian and M. A. El-Sayed, *J. Am. Chem. Soc.*, 2006, **128**, 2115–2120.
42 B. Nikoobakht and M. A. El-Sayed, *Chem. Mater.*, 2003, **15**, 1957–1962.
43 K. N. L. Hoang, S. M. McClain, S. M. Meyer, C. A. Jalomo, N. B. Forney and C. J. Murphy, *Chem. Commun.*, 2022, **58**, 9728–9741.
44 T. Wiseman, S. Williston, J. F. Brandts and L.-N. Lin, *Analytical Biochemistry*, 1989, **179**, 131–137.
45 A. Brown, *Int J Mol Sci*, 2009, **10**, 3457–3477.
46 A. Velazquez-Campoy, G. Goñi, J. R. Peregrina and M. Medina, *Biophys J*, 2006, **91**, 1887–1904.
47 B. W. Sigurskjold, *Anal Biochem*, 2000, **277**, 260–266.
48 M. W. Freyer and E. A. Lewis, *Methods Cell Biol.*, 2008, **84**, 79–113.
49 N. Grossoehme, A. Spuches and D. Wilcox, *Journal of Biological Inorganic Chemistry*, 2010, **15**, 1183–1191.
50 C. F. Quinn, M. C. Carpenter, M. L. Croteau and D. E. Wilcox, in *Methods in Enzymology*, ed. A. L. Feig, Academic Press, 2016, vol. 567, pp. 3–21.
51 D. Prozeller, S. Morsbach and K. Landfester, *Nanoscale*, 2019, **11**, 19265–19273.
52 K. A. Nguyen, R. Pachter and P. N. Day, *J. Phys. Chem. A*, 2020, **124**, 10472–10481.
53 J. R. Lakowicz, *Principles of Fluorescence Spectroscopy*, Springer, New York, 3rd edn., 2006.
54 I. Moreels, J. C. Martins and Z. Hens, *ChemPhysChem*, 2006, **7**, 1028–1031.
55 E. S. Williams, K. J. Major, A. Tobias, D. Woodall, V. Morales, C. Lippincott, P. J. Moyer and M. Jones, *J. Phys. Chem. C*, 2013, **117**, 4227–4237.
56 J. H. Dunlap, N. P. Jayaweera, P. J. Pellechia and A. B. Greytak, *J. Phys. Chem. C*, 2022, **126**, 17635–17646.
57 S. L. Abiodun, M. Y. Gee and A. B. Greytak, *J. Phys. Chem. C*, 2021, **125**, 17897–17905.
58 M. Y. Gee, PhD Thesis, University of South Carolina, 2019.
59 M. Y. Gee, Y. Shen and A. B. Greytak, *J. Phys. Chem. C*, 2020, **124**, 23964–23975.
60 O. Elimelech, O. Aviv, M. Oded and U. Banin, *Nano Lett.*, 2020, **20**, 6396–6403.
61 O. Elimelech, O. Aviv, M. Oded, X. Peng, D. Harries and U. Banin, *ACS Nano*, 2022, **16**, 4308–4321.
62 J. J. Calvin, E. A. O'Brien, A. B. Sedlak, A. D. Balan and A. P. Alivisatos, *ACS Nano*, 2021, **15**, 1407–1420.

63 J. J. Calvin, A. Ben-Moshe, E. B. Curling, A. S. Brewer, A. B. Sedlak, T. M. Kaufman and A. P. Alivisatos, *J. Phys. Chem. C*, 2022, **126**, 12958–12971.
64 V. Ravi, J. M. Binz and R. M. Rioux, *Nano Lett.*, 2013, **13**, 4442–4448.
65 S. Jharimune, A. A. Sathe and R. M. Rioux, *Nano Lett.*, 2018, **18**, 6795–6803.
66 S. Mondal, D. Ghosh, C. N. Roy and A. Saha, *RSC Adv.*, 2014, **4**, 13085–13092.
67 Y. Shen, R. Tan, M. Y. Gee and A. B. Greytak, *ACS Nano*, 2015, **9**, 3345–3359.
68 B. A. Pethica, *Anal. Biochem.*, 2015, **472**, 21–29.
69 L. D. Hansen, G. W. Fellingham and D. J. Russell, *Anal Biochem*, 2011, **409**, 220–229.
70 E. Freire, A. Schön and A. Velazquez-Campoy, in *Biothermodynamics, Part A*, eds. M. L. Johnson, J. M. Holt and G. K. Ackers, Academic Press, 2009, vol. 455, pp. 127–155.
71 C. A. Brautigam, *Methods*, 2015, **76**, 124–136.
72 J. J. Calvin, J. K. Swabeck, A. B. Sedlak, Y. Kim, E. Jang and A. P. Alivisatos, *J. Am. Chem. Soc.*, 2020, **142**, 18897–18906.
73 L. Wadsö, Y. Li and X. Li, *J. Chem. Educ.*, 2011, **88**, 101–105.
74 D. E. Moore, D. R. Goode, C. S. Seney and J. M. Boatwright, *J. Chem. Educ.*, 2016, **93**, 304–310.
75 A. M.-P. Pederson, E. M. Ward, D. V. Schoonover, C. Slebodnick and H. W. Gibson, *J. Org. Chem.*, 2008, **73**, 9094–9101.
76 N. Markova and D. Hallén, *Anal Biochem*, 2004, **331**, 77–88.
77 J. W. Chang, A. Armaou and R. M. Rioux, *J. Phys. Chem. B*, 2021, **125**, 8075–8087.
78 E. A. Weiss, *Acc. Chem. Res.*, 2013, **46**, 2607–2615.
79 C. Giansante, *Acc. Chem. Res.*, 2020, **53**, 1458–1467.
80 M. V. Kovalenko, M. Scheele and D. V. Talapin, *Science*, 2009, **324**, 1417–1420.
81 M. Green, *J. Organomet. Chem.*, 1995, **500**, 127–148.
82 P. E. Chen, N. C. Anderson, Z. M. Norman and J. S. Owen, *J. Am. Chem. Soc.*, 2017, **139**, 3227–3236.
83 N. P. Jayaweera, J. H. Dunlap, F. Ahmed, T. Larison, L. Buzoglu Kurnaz, M. Stefik, P. J. Pellechia, A. W. Fountain and A. B. Greytak, *Inorg. Chem.*, 2022, **61**, 10942–10949.
84 J. De Roo, M. Ibáñez, P. Geiregat, G. Nedelcu, W. Walravens, J. Maes, J. C. Martins, I. Van Driessche, M. V. Kovalenko and Z. Hens, *ACS Nano*, 2016, **10**, 2071–2081.
85 M. I. Bodnarchuk, S. C. Boehme, S. ten Brinck, C. Bernasconi, Y. Shynkarenko, F. Krieg, R. Widmer, B. Aeschlimann, D. Günther, M. V. Kovalenko and I. Infante, *ACS Energy Lett.*, 2019, **4**, 63–74.
86 S. R. Smock, T. J. Williams and R. L. Brutchey, *Angewandte Chemie*, 2018, **130**, 11885–11889.
87 Y. Chen, S. R. Smock, A. H. Flintgruber, F. A. Perras, R. L. Brutchey and A. J. Rossini, *J. Am. Chem. Soc.*, 2020, **142**, 6117–6127.
88 M. Imran, P. Ijaz, L. Goldoni, D. Maggioni, U. Petralanda, M. Prato, G. Almeida, I. Infante and L. Manna, *ACS Energy Lett.*, 2019, **4**, 819–824.
89 S. L. Abiodun, P. J. Pellechia and A. B. Greytak, *J. Phys. Chem. C*, 2021, **125**, 3463–3471.
90 M. Liu, Y.-Y. Wang, Y. Liu and F.-L. Jiang, *J. Phys. Chem. C*, 2020, **124**, 4613–4625.
91 J. Zito and I. Infante, *Acc. Chem. Res.*, 2021, **54**, 1555–1564.
92 C. B. Murray, D. J. Norris and M. G. Bawendi, *Journal of the American Chemical Society*, 1993, **115**, 8706–8715.
93 S. Christodoulou, G. Vaccaro, V. Pinchetti, F. D. Donato, J. Q. Grim, A. Casu, A. Genovese, G. Vicidomini, A. Diaspro, S. Brovelli, L. Manna and I. Moreels, *J. Mater. Chem. C*, 2014, **2**, 3439–3447.
94 A. B. Greytak, P. M. Allen, W. Liu, J. Zhao, E. R. Young, Z. Popović, B. J. Walker, D. G. Nocera and M. G. Bawendi, *Chem. Sci.*, 2012, **3**, 2028–2034.
95 M. A. Hines and G. D. Scholes, *Adv. Mater.*, 2003, **15**, 1844–1849.
96 A. Aharoni, T. Mokari, I. Popov and U. Banin, *J. Am. Chem. Soc.*, 2006, **128**, 257–264.
97 J. Zhang, R. W. Crisp, J. Gao, D. M. Kroupa, M. C. Beard and J. M. Luther, *J. Phys. Chem. Lett.*, 2015, **6**, 1830–1833.
98 D. E. Westmoreland, R. López-Arteaga and E. A. Weiss, *J. Am. Chem. Soc.*, 2020, **142**, 2690–2696.
99 E. T. Vickers, E. E. Enlow, W. G. Delmas, A. C. DiBenedetto, A. H. Chowdhury, B. Bahrami, B. W. Dreskin, T. A. Graham, I. N. Hernandez, S. A. Carter, S. Ghosh, Q. Qiao and J. Z. Zhang, *ACS Energy Lett.*, 2020, **5**, 817–825.
100 E. T. Vickers, T. A. Graham, A. H. Chowdhury, B. Bahrami, B. W. Dreskin, S. Lindley, S. B. Naghadeh, Q. Qiao and J. Z. Zhang, *ACS Energy Lett.*, 2018, **3**, 2931–2939.
101 N. C. Anderson and J. S. Owen, *Chem. Mater.*, 2013, **25**, 69–76.
102 J. Pan, L. N. Quan, Y. Zhao, W. Peng, B. Murali, S. P. Sarmah, M. Yuan, L. Sinatra, N. M. Alyami, J. Liu, E. Yassitepe, Z. Yang, O. Voznyy, R. Comin, M. N. Hedhili, O. F. Mohammed, Z. H. Lu, D. H. Kim, E. H. Sargent and O. M. Bakr, *Advanced Materials*, 2016, **28**, 8718–8725.
103 C. R. Kagan and C. B. Murray, *Nature Nanotech*, 2015, **10**, 1013–1026.
104 D. M. Kroupa, M. Vörös, N. P. Brawand, B. W. McNichols, E. M. Miller, J. Gu, A. J. Nozik, A. Sellinger, G. Galli and M. C. Beard, *Nat Commun*, , DOI:10.1038/ncomms15257.
105 M. Yu, Y. Yang, R. Han, Q. Zheng, L. Wang, Y. Hong, Z. Li and Y. Sha, *Langmuir*, 2010, **26**, 8534–8539.
106 J. H. Dunlap, A. F. Loszko, R. A. Flake, Y. Huang, B. C. Benicewicz and A. B. Greytak, *J. Phys. Chem. C*, 2018, **122**, 26756–26763.
107 M. Tasso, E. Giovanelli, D. Zala, S. Bouccara, A. Fragola, M. Hanafi, Z. Lenkei, T. Pons and N. Lequeux, *ACS Nano*, 2015, **9**, 11479–11489.
108 E. Muro, T. Pons, N. Lequeux, A. Fragola, N. Sanson, Z. Lenkei and B. Dubertret, *J. Am. Chem. Soc.*, 2010, **132**, 4556–4557.
109 J. Ye, M. M. Byranvand, C. O. Martínez, R. L. Z. Hoye, M. Saliba and L. Polavarapu, *Angewandte Chemie*, 2021, **133**, 21804–21828.
110 R. Sliz, M. Lejay, J. Z. Fan, M.-J. Choi, S. Kinge, S. Hoogland, T. Fabritius, F. P. García de Arquer and E. H. Sargent, *ACS Nano*, 2019, **13**, 11988–11995.
111 M. L. Kelley, F. Ahmed, S. L. Abiodun, M. Usman, M. U. Jewel, K. Hussain, H.-C. zur Loye, M. V. S. Chandrashekhar and A. B. Greytak, *ACS Appl. Electron. Mater.*, 2021, **3**, 1550–1555.
112 K. S. Jeong, J. Tang, H. Liu, J. Kim, A. W. Schaefer, K. Kemp, L. Levina, X. Wang, S. Hoogland, R. Debnath, L. Brzozowski, E. H. Sargent and J. B. Asbury, *ACS Nano*, 2012, **6**, 89–99.
113 M.-J. Choi, F. P. García de Arquer, A. H. Proppe, A. Seifitokaldani, J. Choi, J. Kim, S.-W. Baek, M. Liu, B. Sun, M. Biondi, B. Scheffel, G. Walters, D.-H. Nam, J. W. Jo, O. Ouellette, O. Voznyy, S. Hoogland, S. O. Kelley, Y. S. Jung and E. H. Sargent, *Nature Communications*, 2020, **11**, 103.
114 W. Liu, A. B. Greytak, J. Lee, C. R. Wong, J. Park, L. F. Marshall, W. Jiang, P. N. Curtin, A. Y. Ting, D. G. Nocera, D. Fukumura, R. K. Jain and M. G. Bawendi, *Journal of the American Chemical Society*, 2010, **132**, 472–483.
115 A. Viswanath, Y. Shen, A. N. Green, R. Tan, A. B. Greytak and B. C. Benicewicz, *Macromolecules*, 2014, **47**, 8137–8144.
116 G. Palui, F. Aldeek, W. Wang and H. Mattoussi, *Chem. Soc. Rev.*, 2014, **44**, 193–227.
117 L. Du, N. A. Nosratabad, Z. Jin, C. Zhang, S. Wang, B. Chen and H. Mattoussi, *J. Am. Chem. Soc.*, 2021, **143**, 1873–1884.

118 Z. Han, S. Sarkar and A. M. Smith, *ACS Nano*, 2020, **14**, 3227–3241.
119 X. Hu, P. Zrazhevskiy and X. Gao, *Ann Biomed Eng*, 2009, **37**, 1960–1966.
120 W. Zheng, Y. Liu, A. West, E. E. Schuler, K. Yehl, R. B. Dyer, J. T. Kindt and K. Salaita, *J. Am. Chem. Soc.*, 2014, **136**, 1992–1999.
121 P. T. Snee, *Accounts Chem. Res.*, 2018, **51**, 2949–2956.
122 M. Zhang, J. Yue, R. Cui, Z. Ma, H. Wan, F. Wang, S. Zhu, Y. Zhou, Y. Kuang, Y. Zhong, D.-W. Pang and H. Dai, *Proc. Natl. Acad. Sci. U.S.A.*, 2018, **115**, 6590–6595.
123 W. Wang, A. Kapur, X. Ji, M. Safi, G. Palui, V. Palomo, P. E. Dawson and H. Mattoussi, *J. Am. Chem. Soc.*, 2015, **137**, 5438–5451.
124 W. Wang, E. A. van Niekerk, Y. Zhang, L. Du, X. Ji, S. Wang, J. D. Baker, K. Groeniger, F. M. Raymo and H. Mattoussi, *Bioconjugate Chem.*, 2020, **31**, 1497–1509.
125 L. Trapiella-Alfonso, T. Pons, N. Lequeux, L. Leleu, J. Grimaldi, M. Tasso, E. Oujagir, J. Seguin, F. d'Orlye, C. Girard, B.-T. Doan and A. Varenne, *ACS Appl. Mater. Interfaces*, 2018, **10**, 17107–17116.
126 V. V. Breus, C. D. Heyes, K. Tron and G. U. Nienhaus, *ACS Nano*, 2009, **3**, 2573–2580.
127 C. Grazon, M. Chern, K. Ward, S. Lecommandoux, M. W. Grinstaff and A. M. Dennis, *Chem. Commun.*, 2019, **55**, 11067–11070.
128 C. M. Johnson, K. M. Pate, Y. Shen, A. Viswanath, R. Tan, B. C. Benicewicz, M. A. Moss and A. B. Greytak, *Journal of Colloid and Interface Science*, 2015, **458**, 310–314.
129 A. Viswanath, P. Paudel, P. Kittikhunnatham, A. N. Green, A. B. Greytak and B. C. Benicewicz, *Polym. Chem.*, 2015, **6**, 7036–7044.
130 K. Malhotra, R. Fuku, T. S. Chan, N. Kraljevic, A. Sedighi, P. A. E. Piunno and U. J. Krull, *Chem. Mater.*, 2020, **32**, 4002–4012.
131 Z. Yang, M. Gao, W. Wu, X. Yang, X. W. Sun, J. Zhang, H.-C. Wang, R.-S. Liu, C.-Y. Han, H. Yang and W. Li, *Mater. Today*, 2019, **24**, 69–93.
132 S. Guldin, S. Hüttner, P. Tiwana, M. Christopher Orilall, B. Ülgüt, M. Stefik, P. Docampo, M. Kolle, G. Divitini, C. Ducati, S. A. T. Redfern, H. J. Snaith, U. Wiesner, D. Eder and U. Steiner, *Energy & Environmental Science*, 2011, **4**, 225–233.
133 A. K. Chakraborty and M. Tirrell, *MRS Bulletin*, 1996, **21**, 28–32.
134 Z. Han, R. M. Vaidya, O. H. Arogundade, L. Ma, M. U. Zahid, S. Sarkar, C.-W. Kuo, P. R. Selvin and A. M. Smith, *Chem. Mater.*, 2022, **34**, 4621–4632.
135 E. Giovanelli, E. Muro, G. Sitbon, M. Hanafi, T. Pons, B. Dubertret and N. Lequeux, *Langmuir*, 2012, **28**, 15177–15184.
136 Z. Xia, E. Villarreal, H. Wang and B. L. T. Lau, *Colloid Surf. B-Biointerfaces*, 2020, **190**, 110960.
137 A. N. Beecher, X. Yang, J. H. Palmer, A. L. LaGrassa, P. Juhas, S. J. L. Billinge and J. S. Owen, *J. Am. Chem. Soc.*, 2014, **136**, 10645–10653.
138 A. Roberge, J. H. Dunlap, F. Ahmed and A. B. Greytak, *Chem. Mater.*, 2020, **32**, 6588–6594.
139 J. Y. Rempel, B. L. Trout, M. G. Bawendi and K. F. Jensen, *J. Phys. Chem. B*, 2006, **110**, 18007–18016.
140 C. L. Hartley and J. L. Dempsey, *Chem. Mater.*, 2021, **33**, 2655–2665.
141 A. B. Greytak, R. Tan and S. K. Roberts, in *Anisotropic and Shape-Selective Nanomaterials: Structure-Property Relationships*, eds. S. E. Hunyadi Murph, G. K. Larsen and K. J. Coopersmith, Springer International Publishing, Cham, 2017, pp. 169–232.
142 E. Lhuillier, S. Pedetti, S. Ithurria, B. Nadal, H. Heuclin and B. Dubertret, *Accounts Chem. Res.*, 2015, **48**, 22–30.
143 H. Choi, J.-H. Ko, Y.-H. Kim and S. Jeong, *J. Am. Chem. Soc.*, 2013, **135**, 5278–5281.
144 B.-K. Pong, B. L. Trout and J.-Y. Lee, *Langmuir*, 2008, **24**, 5270–5276.
145 P. R. Brown, D. Kim, R. R. Lunt, N. Zhao, M. G. Bawendi, J. C. Grossman and V. Bulović, *ACS Nano*, 2014, **8**, 5863–5872.
146 P. B. Green, F. Yarur Villanueva, C. J. Imperiale, M. Hasham, K. Z. Demmans, D. C. Burns and M. W. B. Wilson, *ACS Appl. Nano Mater.*, 2021, **4**, 5655–5664.
147 M. L. Kessler, J. E. Kelm, H. E. Starr, E. N. Cook, J. D. Miller, N. A. Rivera, H. Hsu-Kim and J. L. Dempsey, *Chem. Mater.*, 2022, **34**, 1710–1721.
148 Y. Yao, G. T. DeKoster and W. E. Buhro, *Chem. Mater.*, 2019, **31**, 4299–4312.
149 N. C. Anderson, M. P. Hendricks, J. J. Choi and J. S. Owen, *J. Am. Chem. Soc.*, 2013, **135**, 18536–18548.
150 N. D. Bronstein, M. S. Martinez, D. M. Kroupa, M. Vörös, H. Lu, N. P. Brawand, A. J. Nozik, A. Sellinger, G. Galli and M. C. Beard, *ACS Nano*, 2019, **13**, 3839–3846.
151 M.-J. Choi, L. K. Sagar, B. Sun, M. Biondi, S. Lee, A. M. Najjariyan, L. Levina, F. P. García de Arquer and E. H. Sargent, *Nano Lett.*, 2021, **21**, 6057–6063.
152 H. Sun and W. E. Buhro, *Chem. Mater.*, 2020, **32**, 5814–5826.
153 Y. Shirasaki, G. J. Supran, M. G. Bawendi and V. Bulovic, *Nat. Photonics*, 2013, **7**, 13–23.
154 D. A. Hanifi, N. D. Bronstein, B. A. Koscher, Z. Nett, J. K. Swabeck, K. Takano, A. M. Schwartzberg, L. Maserati, K. Vandewal, Y. van de Burgt, A. Salleo and A. P. Alivisatos, *Science*, 2019, **363**, 1199–1202.
155 M. Cirillo, F. Strubbe, K. Neyts and Z. Hens, *ACS Nano*, 2011, **5**, 1345–1352.
156 J. Owen, *Science*, 2015, **347**, 615–616.
157 A. Ritchhart and B. M. Cossairt, *Inorg. Chem.*, 2019, **58**, 2840–2847.
158 M. L. Kelley, F. Ahmed, S. L. Abiodun, M. Usman, M. U. Jewel, K. Hussain, H.-C. zur Loye, M. V. S. Chandrashekhar and A. B. Greytak, *ACS Appl. Electron. Mater.*, 2021, **3**, 1550–1555.
159 W. Liu, H. S. Choi, J. P. Zimmer, E. Tanaka, J. V. Frangioni and M. Bawendi, *J. Am. Chem. Soc.*, 2007, **129**, 14530–14531.
160 D. E. Westmoreland, R. J. Nap, F. Arcudi, I. Szleifer and E. A. Weiss, *Chem. Commun.*, 2019, **55**, 5435–5438.
161 F. Arcudi, D. E. Westmoreland and E. A. Weiss, *Chemistry – A European Journal*, 2019, **25**, 14469–14474.
162 P. Kuzmic, in *Methods in Enzymology: Computer Methods, Part B*, eds. M. L. Johnson and L. Brand, Elsevier Academic Press Inc, San Diego, 2009, vol. 467, pp. 247–280.
163 R. Gomes, A. Hassinen, A. Szczygiel, Q. Zhao, A. Vantomme, J. C. Martins and Z. Hens, *J. Phys. Chem. Lett.*, 2011, **2**, 145–152.
164 J. De Roo, N. Yazdani, E. Drijvers, A. Lauria, J. Maes, J. S. Owen, I. Van Driessche, M. Niederberger, V. Wood, J. C. Martins, I. Infante and Z. Hens, *Chem. Mater.*, 2018, **30**, 5485–5492.
165 R. Grisorio, M. E. D. Clemente, E. Fanizza, I. Allegretta, D. Altamura, M. Striccoli, R. Terzano, C. Giannini, M. Irimia-Vladu and G. P. Suranna, *Nanoscale*, 2019, **11**, 986–999.
166 Z. Hens and J. C. Martins, *Chem. Mater.*, 2013, **25**, 1211–1221.
167 C. Morrison, H. Sun, Y. Yao, R. A. Loomis and W. E. Buhro, *Chem. Mater.*, 2020, **32**, 1760–1768.
168 A. Striolo, J. Ward, J. M. Prausnitz, W. J. Parak, D. Zanchet, D. Gerion, D. Milliron and A. P. Alivisatos, *J. Phys. Chem. B*, 2002, **106**, 5500–5505.
169 R. R. Knauf, J. C. Lennox and J. L. Dempsey, *Chem. Mater.*, 2016, **28**, 4762–4770.
170 Y. Shen, M. Y. Gee, R. Tan, P. J. Pellechia and A. B. Greytak, *Chem. Mater.*, 2013, **25**, 2838–2848.
171 C. Vinegoni, P. F. Feruglio, I. Gryczynski, R. Mazitschek and R. Weissleder, *Adv Drug Deliv Rev*, 2019, **151–152**, 262–288.

172 M. T. Morgan, A. Maiti, M. E. Fitzgerald and A. C. Drohat, *Nucleic Acids Research*, 2011, **39**, 2319–2329.
173 G. A. Baker, T. A. Betts and S. Pandey, *J. Chem. Educ.*, 2001, **78**, 1100.
174 C. M. Ingersoll and C. M. Strollo, *J. Chem. Educ.*, 2007, **84**, 1313.
175 I. Hadar, T. Abir, S. Halivni, A. Faust and U. Banin, *Angewandte Chemie International Edition*, 2015, **54**, 12463–12467.
176 D. S. Karpovich and G. J. Blanchard, *Langmuir*, 1996, **12**, 5522–5524.
177 A. Sillen and Y. Engelborghs, *Photochemistry and Photobiology*, 1998, **67**, 475–486.
178 X. Li, V. M. Nichols, D. Zhou, C. Lim, G. S. H. Pau, C. J. Bardeen and M. L. Tang, *Nano Lett.*, 2014, **14**, 3382–3387.
179 C. Bullen and P. Mulvaney, *Langmuir*, 2006, **22**, 3007–3013.
180 A. M. Munro, I. Jen-La Plante, M. S. Ng and D. S. Ginger, *J. Phys. Chem. C*, 2007, **111**, 6220–6227.
181 A. J. Morris-Cohen, M. T. Frederick, L. C. Cass and E. A. Weiss, *J. Am. Chem. Soc*, 2011, **133**, 10146–10154.
182 A. J. Morris-Cohen, V. Vasilenko, V. A. Amin, M. G. Reuter and E. A. Weiss, *ACS Nano*, 2011, **6**, 557–565.
183 X. Ji, D. Copenhaver, C. Sichmeller and X. Peng, *J. Am. Chem. Soc.*, 2008, **130**, 5726–5735.
184 N. Phromsiri, S. L. Abiodun, C. Manipuntee, P. Leeladee, A. B. Greytak and N. Insin, *Journal of Molecular Structure*, 2023, **1271**, 134050.
185 A. M. Munro and D. S. Ginger, *Nano Lett.*, 2008, **8**, 2585–2590.
186 L. Khavrutskii, J. Yeh, O. Timofeeva, S. G. Tarasov, S. Pritt, K. Stefanisko and N. Tarasova, *J Vis Exp*, 2013, 50541.
187 M. Jerabek-Willemsen, T. André, R. Wanner, H. M. Roth, S. Duhr, P. Baaske and D. Breitsprecher, *Journal of Molecular Structure*, 2014, **1077**, 101–113.
188 S. A. I. Seidel, P. M. Dijkman, W. A. Lea, G. van den Bogaart, M. Jerabek-Willemsen, A. Lazic, J. S. Joseph, P. Srinivasan, P. Baaske, A. Simeonov, I. Katritch, F. A. Melo, J. E. Ladbury, G. Schreiber, A. Watts, D. Braun and S. Duhr, *Methods*, 2013, **59**, 301–315.
189 C. J. Wienken, P. Baaske, U. Rothbauer, D. Braun and S. Duhr, *Nature Communications*, 2010, **1**, 100.
190 A. Stinn, J. Furkert, S. H. E. Kaufmann, P. Moura-Alves and M. Kolbe, *Biosensors*, 2021, **11**, 60.
191 Y. Shen, M. Y. Gee and A. B. Greytak, *Chem. Commun.*, 2017, **53**, 827–841.
192 T. Kim, M. L. Kelley, D. Kim, A. B. Greytak and S. Jeong, *Int. J. of Precis. Eng. and Manuf.-Green Tech.*, 2021, **8**, 1309–1321.
193 Y. Shen, A. Roberge, R. Tan, M. Y. Gee, D. C. Gary, Y. Huang, D. A. Blom, B. C. Benicewicz, B. M. Cossairt and A. B. Greytak, *Chemical Science*, 2016, **7**, 5671–5679.
194 K. Davis, B. Qi, M. Witmer, C. L. Kitchens, B. A. Powell and O. T. Mefford, *Langmuir*, 2014, **30**, 10918–10925.
195 K. Prather, J. T. Stoffel and E. Y. Tsui, *Chem. Mat.*, 2022, **34**, 3976–3984.
196 C. A. Leatherdale, W.-K. Woo, F. V. Mikulec and M. G. Bawendi, *J. Phys. Chem. B*, 2002, **106**, 7619–7622.
197 J. Jasieniak, L. Smith, J. van Embden, P. Mulvaney and M. Califano, *The Journal of Physical Chemistry C*, 2009, **113**, 19468–19474.
198 W. W. Yu, L. Qu, W. Guo and X. Peng, *Chem. Mater.*, 2003, **15**, 2854–2860.
199 J. Li, J. Chen, Y. Shen and X. Peng, *Nano Res.*, 2018, **11**, 3991–4004.
200 M. Booth, A. P. Brown, S. D. Evans and K. Critchley, *Chem. Mater.*, 2012, **24**, 2064–2070.
201 J. Maes, L. Balcaen, E. Drijvers, Q. Zhao, J. De Roo, A. Vantomme, F. Vanhaecke, P. Geiregat and Z. Hens, *J. Phys. Chem. Lett.*, 2018, **9**, 3093–3097.
202 S. Mannar, P. Mandal, A. Roy and R. Viswanatha, *J. Phys. Chem. Lett.*, 2022, **13**, 6290–6297.
203 T. Rajh, O. I. Micic and A. J. Nozik, *J. Phys. Chem.*, 1993, **97**, 11999–12003.
204 J. S. Kamal, A. Omari, K. Van Hoecke, Q. Zhao, A. Vantomme, F. Vanhaecke, R. K. Capek and Z. Hens, *J. Phys. Chem. C*, 2012, **116**, 5049–5054.
205 I. Moreels, K. Lambert, D. De Muynck, F. Vanhaecke, D. Poelman, J. C. Martins, G. Allan and Z. Hens, *Chem. Mater.*, 2007, **19**, 6101–6106.
206 Q. Dai, Y. Wang, X. Li, Y. Zhang, D. J. Pellegrino, M. Zhao, B. Zou, J. Seo, Y. Wang and W. W. Yu, *ACS Nano*, 2009, **3**, 1518–1524.
207 I. Moreels, K. Lambert, D. Smeets, D. De Muynck, T. Nollet, J. C. Martins, F. Vanhaecke, A. Vantomme, C. Delerue, G. Allan and Z. Hens, *ACS Nano*, 2009, **3**, 3023–3030.
208 L. Cademartiri, J. Bertolotti, R. Sapienza, D. S. Wiersma, G. von Freymann and G. A. Ozin, *J. Phys. Chem. B*, 2006, **110**, 671–673.
209 P. Yu, M. C. Beard, R. J. Ellingson, S. Ferrere, C. Curtis, J. Drexler, F. Luiszer and A. J. Nozik, *J. Phys. Chem. B*, 2005, **109**, 7084–7087.
210 M. Kuno, I. Gushchina, S. Toso and V. Trepalin, *J. Phys. Chem. C*, 2022, **126**, 11867–11874.
211 A. Velazquez-Campoy, *J Therm Anal Calorim*, 2015, **122**, 1477–1483.
212 J. Tellinghuisen, *Analytical Biochemistry*, 2008, **373**, 395–397.
213 L. Fabbrizzi, N. Marcotte, F. Stomeo and A. Taglietti, *Angewandte Chemie International Edition*, 2002, **41**, 3811–3814.
214 A. Roberge, J. L. Stein, Y. Shen, B. M. Cossairt and A. B. Greytak, *J. Phys. Chem. Lett.*, 2017, **8**, 4055–4060.
215 I. Fedin and D. V. Talapin, *J. Am. Chem. Soc.*, 2014, **136**, 11228–11231.
216 E. Drijvers, J. De Roo, J. C. Martins, I. Infante and Z. Hens, *Chem. Mater.*, 2018, **30**, 1178–1186.
217 J. Zhang, H. Zhang, W. Cao, Z. Pang, J. Li, Y. Shu, C. Zhu, X. Kong, L. Wang and X. Peng, *J. Am. Chem. Soc.*, 2019, **141**, 15675–15683.
218 C. D. Bain and G. M. Whitesides, *Angewandte Chemie International Edition in English*, 1989, **28**, 506–512.
219 N. C. Anderson, P. E. Chen, A. K. Buckley, J. De Roo and J. S. Owen, *J. Am. Chem. Soc.*, 2018, **140**, 7199–7205.
220 Y. Wang, A. A. Chen, K. P. Balto, Y. Xie, J. S. Figueroa, T. A. Pascal and A. R. Tao, *ACS Nano*, 2022, **16**, 12747–12754.
221 B. Heyne, K. Arlt, A. Geßner, A. F. Richter, M. Döblinger, J. Feldmann, A. Taubert and A. Wedel, *Nanomaterials*, 2020, **10**, 1858.
222 R. I. Masel, *Principles of adsorption and reaction on solid surfaces*, John Wiley & Sons, Inc., New York, 1996.
223 D. Quarta, M. Imran, A.-L. Capodilupo, U. Petralanda, B. van Beek, F. De Angelis, L. Manna, I. Infante, L. De Trizio and C. Giansante, *J. Phys. Chem. Lett.*, 2019, **10**, 3715–3726.
224 D. M. Kroupa, N. C. Anderson, C. V. Castaneda, A. J. Nozik and M. C. Beard, *Chem. Commun.*, 2016, **52**, 13893–13896.
225 A. Velázquez-Campoy, *Analytical Biochemistry*, 2006, **348**, 94–104.
226 D. Zherebetskyy, M. Scheele, Y. Zhang, N. Bronstein, C. Thompson, D. Britt, M. Salmeron, P. Alivisatos and L.-W. Wang, *Science*, 2014, **344**, 1380–1384.
227 A. K. Chakraborty and A. J. Golumbfskie, *Annual Review of Physical Chemistry*, 2001, **52**, 537–573.
228 P. F. Almeida, *Langmuir*, 2019, **35**, 21–40.
229 D. D. Lovingood, R. Achey, A. K. Paravastu and G. F. Strouse, *J. Am. Chem. Soc.*, 2010, **132**, 3344–3354.

230M. G. Berrettini, G. Braun, J. G. Hu and G. F. Strouse, *J. Am. Chem. Soc.*, 2004, **126**, 7063–7070.
231Y. Chen, R. W. Dorn, M. P. Hanrahan, L. Wei, R. Blome-Fernández, A. M. Medina-Gonzalez, M. A. S. Adamson, A. H. Flintgruber, J. Vela and A. J. Rossini, *J. Am. Chem. Soc.*, 2021, **143**, 8747–8760.
232O. Voznyy, *J. Phys. Chem. C*, 2011, **115**, 15927–15932.
233M. Liu, F. Che, B. Sun, O. Voznyy, A. Proppe, R. Munir, M. Wei, R. Quintero-Bermudez, L. Hu, S. Hoogland, A. Mandelis, A. Amassian, S. O. Kelley, F. P. García de Arquer and E. H. Sargent, *ACS Energy Lett.*, 2019, **4**, 1225–1230.
234F. Bertolotti, D. N. Dirin, M. Ibáñez, F. Krumeich, A. Cervellino, R. Frison, O. Voznyy, E. H. Sargent, M. V. Kovalenko, A. Guagliardi and N. Masciocchi, *Nature Materials*, 2016, **15**, 987.
235A. H. Ip, S. M. Thon, S. Hoogland, O. Voznyy, D. Zhitomirsky, R. Debnath, L. Levina, L. R. Rollny, G. H. Carey, A. Fischer, K. W. Kemp, I. J. Kramer, Z. Ning, A. J. Labelle, K. W. Chou, A. Amassian and E. H. Sargent, *Nat Nano*, 2012, **7**, 577–582.
236N. Geva, J. J. Shepherd, L. Nienhaus, M. G. Bawendi and T. Van Voorhis, *J. Phys. Chem. C*, 2018, **122**, 26267–26274.
237C. Giansante and I. Infante, *J. Phys. Chem. Lett.*, 2017, **8**, 5209–5215.
238A. J. Houtepen, Z. Hens, J. S. Owen and I. Infante, *Chem. Mater.*, 2017, **29**, 752–761.
239M. P. Campos, J. D. Roo, M. W. Greenberg, B. M. McMurtry, M. P. Hendricks, E. Bennett, N. Saenz, M. Y. Sfeir, B. Abécassis, S. K. Ghose and J. S. Owen, *Chem. Sci.*, 2022, **13**, 4555–4565.
240S. K. Balakrishnan and P. V. Kamat, *Chem. Mater.*, 2018, **30**, 74–78.
241H. Takeuchi, B. Omogo and C. D. Heyes, *Nano Lett*, 2013, **13**, 4746–4752.
242W. Xiao, P. Legros, P. Chevallier, J. Lagueux, J. K. Oh and M.-A. Fortin, *ACS Appl. Nano Mater.*, 2018, **1**, 894–907.
243S. J. Rosenthal, *ACS Chem. Neurosci.*, 2019, **10**, 30–32.
244J. D. Marshall and M. J. Schnitzer, *ACS Nano*, 2013, **7**, 4601–4609.
245J. A. Kloepfer, N. Cohen and J. L. Nadeau, *J. Phys. Chem. B*, 2004, **108**, 17042–17049.
246T. Mokari, E. Rothenberg, I. Popov, R. Costi and U. Banin, *Science*, 2004, **304**, 1787–1790.
247K. Chiad, S. H. Stelzig, R. Gropeanu, T. Weil, M. Klapper and K. Müllen, *Macromolecules*, 2009, **42**, 7545–7552.
248N. Gal, M. Schroffenegger and E. Reimhult, *The Journal of Physical Chemistry B*, 2018, **122**, 5820–5834.
249N. S. Leitner, M. Schroffenegger and E. Reimhult, *ACS Appl. Bio Mater.*, 2021, **4**, 795–806.
250J. M. de la Fuente, P. Eaton, A. G. Barrientos, M. Menéndez and S. Penadés, *J. Am. Chem. Soc.*, 2005, **127**, 6192–6197.
251M. De, C.-C. You, S. Srivastava and V. M. Rotello, *J. Am. Chem. Soc.*, 2007, **129**, 10747–10753.
252G. Y. Tonga, Y. Jeong, B. Duncan, T. Mizuhara, R. Mout, R. Das, S. T. Kim, Y.-C. Yeh, B. Yan, S. Hou and V. M. Rotello, *Nature Chem*, 2015, **7**, 597–603.
253J. S. Owen, J. Park, P.-E. Trudeau and A. P. Alivisatos, *J. Am. Chem. Soc.*, 2008, **130**, 12279–12281.

Graphical abstract / Table of Contents image:

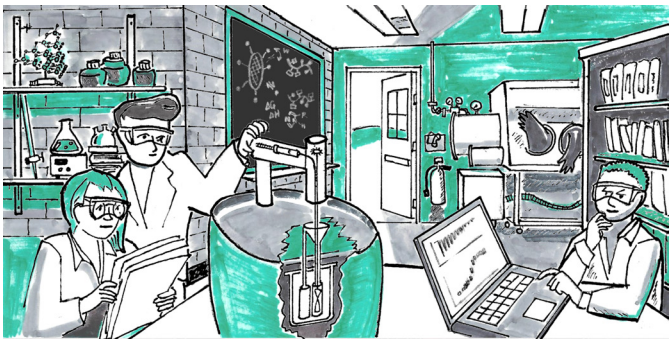

Fundamentals and recent results in the use of ITC to study nanocrystal surfaces, but also emphasizes thermodynamic models independently of techniques. Coordination chemistry common to NC quantum dots, alternative methods, and outlook are discussed.